THE REPUBLIC OF TURKEY
BAHCESEHIR UNIVERSITY

ITERATIVE LEARNING CONTROLLER FOR THE REDUCTION OF COMMUTATION TORQUE RIPPLES IN BRUSHLESS DC MOTOR DRIVES

Master's Thesis

IHSAN OBAYES KHUDHAIR KHUDHAIR

ISTANBUL, 2015

THE REPUBLIC OF TURKEY
BAHCESEHIR UNIVERSITY

GRADUATE SCHOOL OF NATURAL AND APPLIED SCIENCES

M.S. PROGRAM IN ELECTRICAL AND ELECTRONICS ENGINEERING

ITERATIVE LEARNING CONTROLLER FOR THE REDUCTION OF COMMUTATION TORQUE RIPPLES IN BRUSHLESS DC MOTOR DRIVES

Master's Thesis

IHSAN OBAYES KHUDHAIR KHUDHAIR

Supervisor: ASSISTANT PROFESSOR, DR. TURKER TURKER

ISTANBUL, 2015

THE REPUBLIC OF TURKEY
BAHÇEŞEHİR UNIVERSITY

GRADUATE SCHOOL OF NATURAL AND APPLIED SCIENCES
ELECTRICAL-ELECTRONICS GRADUATE PROGRAM

Name of the thesis: Iterative Learning Controller for the Reduction of Commutation Torque Ripples in Brushless DC Motor Drives
Name/Last Name of the Student: Ihsan Obayes Khudhair Khudhair
Date of the Defense of Thesis: 02.06.2015

The thesis has been approved by the Graduate School of Natural and Applied Sciences.

Associate Prof., Nafiz ARICA
Graduate School Director
Signature

I certify that this thesis meets all the requirements as a thesis for the degree of Master of Sciences.

Assistant Prof., Ayça YALÇIN ÖZKUMUR
Program Coordinator
Signature

This is to certify that we have read this thesis and we find it fully adequate in scope, quality and content, as a thesis for the degree of Master of Sciences.

Examining Comittee Members	Signature
Thesis Supervisor Assistant Prof., Türker TÜRKER	
Member Assistant Prof., Yalçın ÇEKİÇ	
Member Assistant Prof., Ali Fuat ERGENÇ	

To spirit of my brother Eng. Erfan

And all my family

ACKNOWLEDGEMENTS

I would like to denote my gratefulness and respect to my advisor Dr. Turker Turker for his help, his guidance and his support. I also like to thank Mr. Fayed Kadhim Jasim for his decision to give me this opportunity to get my master degree. I wish to extend my thanks to Mr. Erdem Erzurum for his help.

Istanbul, 2015 Ihsan Obayes Khudhair Khudhair

ABSTRACT

ITERATIVE LEARNING CONTROLLER FOR THE REDUCTION OF COMMUTATION TORQUE RIPPLES IN BRUSHLESS DC MOTOR DRIVES

Ihsan Obayes Khudhair khudhair

Electrical and Electronics Engineering

Supervisor: Assistant professor Dr. Turker Turker

June 2015, 72 Pages

Brushless DC motors have many advantages such as high power density, easy to control, high ratio of torque/inertia, high ratio of power/weight and long operational life. But there is an undesirable effect seen in BLDC motors which is the torque ripple. Torque ripple is one of the major reasons restricting BLDC motor for the applications requiring high performance.

This study deals with the torque ripples in BLDC motors, especially with the torque ripple that is generated during the commutation period. The analysis of the reasons of commutation torque ripple has performed and some methods have been proposed to reduce the commutation torque ripples in the literature. Conventional proportional integral (PI) controllers are widely used as a controller for permanent magnets motors due to their easy application and simple control formation. However these traditional controllers need precise linear models. Therefore, they are not suitable for BLDC motors because of the nonlinearities in their dynamical model.

When a controller applied to BLDC motors, the error signals are gathered from previous steps have much information which may be used to get high and fast performance. But in conventional control system, they are generally unused and neglected. On the other hand, there are other controllers which track and use these signal in order to get fast performance. One of these control structures is called Iterative Learning Controller. In

this work, a method is proposed to reduce the commutation torque ripple by using a combination of Iterative Learning Controller (ILC) and conventional dead-beat controller. ILC tracks previous errors occurred in commutation period and compensate them in next steps. Usage of gathered error signals is useful to improve the effectiveness of control system in order to suppress torque ripple. The characteristics of this controller are evaluated by numerical simulation, based on the mathematical equations of the brushless DC motor. The results of the proposed controller show that the torque ripples during commutation period are attenuated.

Keywords: Commutation Torque Ripple, BLDC Motors, Iterative Learning Controller

ÖZET

FIRÇASIZ DOĞRU AKIM MOTORLARINDA KOMUTASYON MOMENT DALGALANMALARININ İNDİRGENEMSİ İÇİN ÖĞRENME TEMELLİ KONTROLCÜ TASARIMI

Ihsan Obayes Khudhair khudhair

Elektrik-Elektronik Mühendisliği

Tez Danışmanı: Yrd.Doç.Dr. Türker Türker

Haziran 2015, 72 sayfa

Fırçasız doğru akım motorları (FDAM) yüksek güç yoğunluğu, kontrolünün kolay olması, yüksek moment/atalet oranı, yüksek güç/ağırlık oranı, uzun kullanım süresi gibi birçok avantaja sahiptir. Fakat FDAM'nda moment dalgalanmaları istenmeyen bir özellik olarak karşımıza çıkmaktadır. Moment dalgalanmaları, yüksek performans istenilen uygulamalar için FDAM'nın kullanımını kısıtlayıcı sebeplerin başında gelmektedir.

Bu çalışmada, FDAM'nda özellikle komütasyon periyodunda karşılaşılan moment dalgalanmaları ile ilgilenilmiştir. Literatürde komütasyon moment dalgalanmalarının sebeplerinin analizi fazlaca çalışılmış ve bu dalgalanmaların indirgenmesi için farklı yöntemler sunulmuştur. Geleneksel PI kontrolcüler kolayca uygulanabilir ve basit yapıya sahip olmaları sebebi ile sabit mıknatıslı motorların kontrolü için çokça kullanılmıştır. Fakat, bu geleneksel kontrolcüler sistemin tam olarak bilinen doğrusal modeline ihtiyaç duyarlar. FDAM'nın dinamik modelinin doğrusal olmayan yapıya sahip olması sebebi ile bu kontrolcüler FDAM için uygun değildirler.

FDAM için bir kontrolcü uygulandığında, önceki adımlarda elde edilen hata sinyali, daha iyi ve hızlı bir performans elde etmek için sonraki adımlarda kullanılmak üzere

birçok bilgi barındırırlar. Fakat geleneksel bir kontrol yönteminde bu bilgi kullanılmaz. Diğer taraftan, performansı arttırmak üzere bu hata sinyallerini izleyen ve kullanan kontrolcüler de mevcuttur. Bu kontrol yapılarından bir tanesi iteratif öğrenme bazlı kontrol yapılarıdır. Bu çalışmada, komütasyon moment dalgalanmalarını indirgemek üzere geleneksel deadbeat kontrolcü ile iteratif öğrenme bazlı kontrolcünün bir birleşimi sunulmaktadır. İteratif öğrenme bazlı kontrol yapısı, önceki komütasyon moment dalgalanmalarını izleyerek sonraki adımlarda oluşan hataları indirgemek üzere sisteme eklenmiştir. Moment dalgalanmalarında iyileştirme sağlayabilmek için, kontrol sisteminin verimliliğini geliştirmek üzere elde edilen hata sinyalleri oldukça kullanışlıdır. Elde edilen kontrolcünün özellikleri FDAM'nın matematiksel denklemleri kullanılarak benzetim çalışmaları ile desteklenmiştir. Önerilen kontrol yapısının sonuçları moment dalgalanmalarında iyileşmeler olduğunu göstermektedir.

Anahtar kelimeler: Komütasyon Moment Dalgalanmaları, FDAM, Iteratif Öğrenme Bazlı Denetim.

CONTENTS

TABLES

FIGURES

ABBREVIATIONS

AC:	Adaptive Controller
AC:	Alternating Current, A
CCF:	Current Cycle Feedback
CNC:	Computer Numerical Control
DC:	Direct Current, A
DVD:	Digital Versatile Disc" or "digital video disc
EMF:	Electromotive Force, V
ILC:	Iterative Learning Controller
PCF:	Previous Cycle Feedback
PMBLDC:	Permanent Magnet Brushless DC Motors
PMM:	Permanent Magnet Motors
PMSM:	Permanent Magnet Synchronous Motors
RPM:	Revelation Per Minute, r/min
RC:	Repetitive Controller
NN:	Neural Networks

SYMBOLS

Angular position of the rotor, rad	:	θ
Angular velocity, rad/ s	:	ω
Current Cycle Feedback Gain	:	r
Delta connection	:	Δ
Derivative gain	:	k_d
Electrical angle, degree	:	θ_e
Electrical angular velocity, rad/s	:	ω_e
Electromagnetic torque, N. m	:	T_e
Error	:	er
Friction coefficient, N. M /rad/sec.	:	B
Induced back (EMF) in coil a, V	:	e_a
Induced back (EMF) in coil b, V	:	e_b
Induced back (EMF) in coil c, V	:	e_c
Induced back (EMF) in outgoing coil, V	:	e_{out}
Inductance of each coil in BLDC motor, H	:	L
Input control signal	:	$u(t)$
Integral gain	:	k_i
Internal radius of the rotor, mm	:	r
Iteration	:	k
Length of the rotor, mm	:	l
Load torque, N. m	:	T_L
Markov parameter	:	γ
Matrix	:	M
Maximum torque, N. m	:	T_{MAX}
Measured current, A	:	i
Minimum Torque, N. m	:	T_{MIN}
Moment of inertia, Kg-m2	:	J
Motor back (EMF) constant, V-sec/rad	:	k_e
Motor speed, RPM	:	W_R

Number of stator's poles	:	P
Number of winding turns per phase	:	N
Outgoing current, A	:	i_{out}
Outgoing voltage, V	:	v_{out}
Period of PWM, Hz	:	T_p
Phase current of coil a in BLDC motor, A	:	i_a
Phase current of coil b in BLDC motor, A	:	i_b
Phase current of coil c in BLDC motor, A	:	i_c
Phase voltage coil a, V	:	v_a
Phase voltage coil b, V	:	v_b
Phase voltage coil c, V	:	v_C
Position function in the induced back (EMF) in phase a	:	f_{a}
Position function in the induced back (EMF) in phase b	:	f_{b}
Position function in the induced back (EMF) in phase c	:	f_{c}
Predicted angle, degree	:	$\hat{\theta}e$
Previous Cycle Feedback Gain	:	Φ
Proportional gain	:	k_p
Ratio	:	ρ
Reference current, A	:	i^*
Reference voltage, V	:	V*
Remaining time of commutation, s	:	T_c
Resistance for each coil in BLDC motor, Ohm	:	R
Rotor magnetic field density	:	B
Star connection	:	λ
State transition matrix	:	A
Steady-state value of the phase current, A	:	I
Time, sec.	:	t
Top width of the waveforms of back (EMF), V	:	E
Torque constant, N. m/A	:	k_t
Voltage between phase a and b, V	:	v_{ab}
Voltage between phase a and c, V	:	v_{ac}

Voltage between phase b and a, V	:	v_{ba}
Voltage between phase b and c, V	:	v_{bc}
Voltage between phase c and a, V	:	v_{ca}
Voltage between phase c and b, V	:	v_{cb}
Voltage between phase a and the midpoint of the inverter, V	:	v_{a_0}
Voltage between phase b and the midpoint of the inverter, V	:	v_{b_0}
Voltage between phase c and the midpoint of the inverter, V	:	v_{c_0}

1. INTRODUCTION

Permanent magnet motors consists of a rotor made from permanent magnets and the stator made from electrical windings (coils) that are excited by supply voltage. These motors have ability to run at constant speed irrespective of changing load acting on, and because of that, these motors have high efficiency and are suitable for many applications. Its stator windings, due to the supply voltage, produce revolving magnetic field which interacts with constant magnetic field that is produced by rotor. That interaction leads to rotate the rotor. These motors can be classified into two types depending on the waveforms of the induced voltage in stator windings:-

1. Permanent magnet synchronous motors (PMSM).
2. Permanent magnet brushless DC motors (PMBLDC or BLDC).

The basic properties and features of the PMSM and BLDC motors are characterized in Table 1.1(Krishnan, R., 2010 & Lee, S. No date).

Table 1.1: The comparison between PMSM and BLDC motor

Feature	PMSM	BLDC
Back (EMF)	Sinusoidal	Trapezoidal
Control	Complex and high cost	Simple and low cost
Supply voltage	AC voltage	DC voltage
Torque	Smooth, weak and its peak is lower	Torque ripple is high
Current	Sinusoidal	Rectangular (ideal)
Rotor position sensor	Encoder or Resolver, high cost	Usually hall effect sensor, low cost
Power density	Lower	Higher
Control requirement	1. Continuous rotor position. 2. Significant vector operation	1. Require only six discrete rotor position. 2. Without significant vector operation

*Source: Krishnan, R., 2010 & Lee, S. No dat*e

In industrial applications almost all types of conventional motors such as AC squirrel cage induction motors, AC slip ring induction motors and Brushed DC motors have been used. Each one of them has advantages and disadvantages but they all share the need to periodic and sudden maintenances. Also they need complex and large shapes of power drivers (AC or DC drivers). For instance, in motorized household devices such as fans, refrigerators, air conditioners, etc., single phase AC motors are widely used. These motors cannot start rotating by themselves, therefore additional parts are used to provide the startup rotation such as centrifugal switch, startup windings and capacitors, which may cause extra maintenance effort and increase malfunction rate. In conventional DC motors, the existence of brushes and commutator (mechanical rectifier) is essential to the commutation (process of change direction of rotor current). That means motors have extra rotating parts and mechanical parts for adjusting (brush holders, springs) and these parts will make the motor's shape bigger as well as the voice of rotation will be high typically. The comparison between conventional DC motors and brushless DC motors is given in Table 1.2.

Table 1.2: The comparison between brushed DC and BLDC motor

Feature	Brush DC	BLDC
Commutation	Mechanical rectifier	Electronic rectifier
Driver and controller	Complex and high cost	Simple and low cost
Supply voltage	DC voltage for armature and field	DC voltage for stator only
Life	Shorter	Longer
Size	Larger and rotor is heavier	Lighter rotor
Noise	High	Silent device
Speed range	Lower (mechanical limitation)	Higher
Control requirement	Without rotor position.	6 discrete rotor position.
Maintenance	Require periodic Maintenance	Less
Torque and effici.	Low	High

Source: Padmaraja, 2013 & Brown, 2002

In industrial applications, a lot of manufacturing processes such as cutting, weighing, packaging, picking and stopping for position or distance need to have accurate stops. Brushed DC motors can be implemented in such applications, but they need curbing devices (brake and clutch) and they are associated with other devices for example pneumatic or hydraulic systems that increase complexity of the control system. Therefore, it requires a complex control system which increases the cost.

BLDC motors have started to enter in many applications such as industrial, household, robots and some aircraft motors**.** In industrial applications, due to the ideal and accurate stops of these motors, they have been used for piking, painting and placing. In aircraft's motors, usage of brushless DC motors has been started for its high efficiency (torque, speed) in spite of its small power as well as the low maintenance.

There are other applications for BLDC motors such as household, aerospace, medical, automotive, computers (DVD drive, cooling fans) and tensioning equipment which need specific torque. The modern life has developed towards low cost and better performance in all its aspects and using brushless DC motors reflects that development. In summary, using of brushless DC motors began growing as a result of several factors: (Lee, J. T, 2014, Lee, E. C, No date and Oguntoyinbo, O. J., 2009)

1. Variable speed ranges.
2. Low noise (silent devices).
3. Good heat dissipates.
4. Long operational life.
5. Low maintenance (almost zero).
6. High efficiency.
7. Easy to control.
8. High ratio of (torque/ inertia).
9. High ratio of (power /weight).
10. High power density.
11. High reliability.
12. They can be worked in flammable process.
13. Feedback device (Hall sensors) is inside the motor not outside.

Brushless DC Motors are permanent magnet motors (PMM) that produce a constant magnetic field in rotor while the winding of the stator produces revolving magnetic field. The frequency of these fields are the same, but the magnetic field of the stator is

in advance angle with the magnetic field of rotor by 90^0 in ideal cases, however the real angle varies between (60^0,120^0) (Berendsen, C-S., 1993).

BLDC motors consist of rotor, stator and sensors. The rotor is made from permanent magnets. Thus, it is different from conventional DC motors where the rotor has the coils energized with electricity. The number of rotor poles varies from 2-10 poles and it will be affected upon the torque ripple and the mechanical revolution per electrical cycle as in Equation 1.1.

$$RPM_{mechanical} = 2 * RPM_{electrical} / \text{Number of poles} \quad \textbf{(1.1)}$$

Therefore, the period of switching between stator windings is repeated more with more poles. In addition to this, since the hall effect sensors produce signal for each electrical revolution, the more number of poles the more accurate signal from hall effect sensors can be obtained. Therefore, the sequence of stator winding switching will be fast due to more poles that gives small steps leading to reduce ripple (Atmel AVR443, 2013). In addition, the permanent magnet rotor in brushless DC motor is lighter than the rotor of the brushed DC motor and has long live operation (Atmel Corporation, 2008). The second part is the stator which is consisted of a number of windings (coils) and each winding separately into two halves. The number of winding classifies motor to 1 phase, 2 phases or 3 phases. They will be connected either star connecting (λ) or delta connecting (Δ). The stator here does what the rotor doing in the conventional DC motors. Depending on the design of stator windings and the DC supply voltage, the electromagnetic force which induced in BLDC's stator windings has trapezoidal waveforms. The number of winding plays major role to produce smooth torque (few ripple), that means motor with 3 phase winding has less torque ripple than the one with 2 or 1 phases. In addition BLDC motor is equivalent to inverse of conventional DC motor which has brushes and commutators. That means, the constant magnetic field from rotor will rotate while the windings remain stationary. But in conventional DC motor the constant field will remain stationary and the revolving magnetic field produced by windings in rotor will rotate (Atmel Corporation, 2008). Figures 1.1and 1.2 indicate stator and rotor of a 2 pole and 4 pole BLDC motor respectively.

Figure 1.1: Stator and Rotor of a 2 pole BLDC Motor

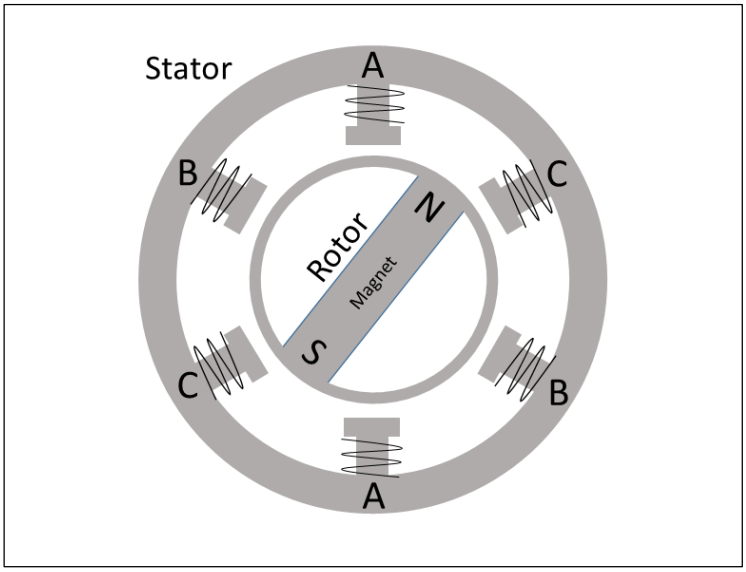

Source: Eriksson, P., 2014

Figure 1.2: Stator and Rotor of a 4 pole BLDC Motor

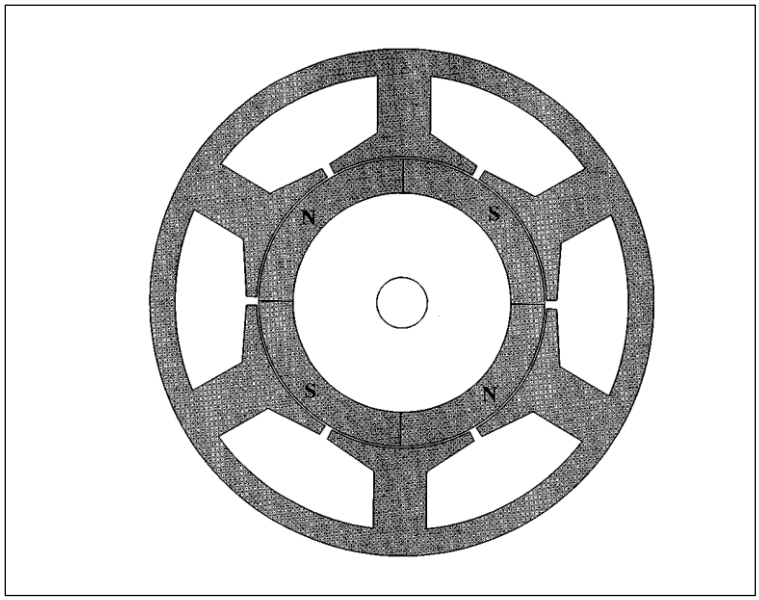

Source: Park, S. J., 2000

Although BLDC motors can be operated sensorless in general, there maybe three sensors installed inside the motor facing the rotor on the non-driving end of the motor. The angle between them is 120^0 (Elevich, L. N., 2005), that means phase shift from each to other is 120^0. According to which pole passing near the sensors south or north

pole, the sensors produce high or low signal voltage. These signals are sent to controller. Thus, the rotor position is exactly known and the controller decides which winding is to be energized with positive voltage, negative voltage or which is not energized. This process is very important to switch the stator winding in the correct sequence at the correct time and it is called commutation (Padmaraja, Y., 2003).

The purpose of this thesis is to design Iterative Learning Controller for brushless DC motor in order to suppress the ripple and pulsation in output torque, especially the commutation torque ripple. Due to high efficiency, high torque in spite of small power and progress in field of magnetic materials, the brushless DC motors (BLDC)s have been widely used in many applications such as Industrial, Aerospace, Robots, etc. The main drawback of these motors is torque ripple. Existence of ripples in torque leads to vibration, noise, speed oscillations and fluctuations thereby defects and deviations in applications. There are some reasons which cause torque ripples. This thesis discusses one of them which is commutation torque ripple by defining it and investigating the reasons for its existence as well as reduce the torque ripple via designing iterative learning controller for the current loop of BLDC motors. The proposed controller is tested through numerical simulations.

The chapter format for thesis is given as below:-

1. Chapter 1 gives brief information to permanent magnets motors, motors' applications, and brushless DC motor.
2. Chapter 2 gives literature review of proposed methods that are used to reduce torque ripples in PWM.
3. Chapter 3 donates the, modeling and mathematical equations of BLDC motor, waveforms of hall effect sensors and electromotive force back (EMF), commutation torque ripple, currents and torque analysis and other reasons for torque ripple. It also gives simple background to iterative learning controller.
4. Chapter 4 indicates how the proposed controller is designed and what the drawback is appeared and its solution as well as the figures and tables of simulation results.
5. Chapter 5 gives concluding remarks of the thesis.

2. LITERATURE REVIEW

There are some proposed methods which are used to attenuate the ripple in output torque for BLDC motors. Some of them are designed for high speed operation, low speed operation and some for full range speed operation. Because of there are several types of torque ripple, each method is specialized for particular type of ripple. Some of them are existed to manipulate and modify the duty cycle of PWM during commutation period in order to equalize time for descent of outgoing current with rise time of incoming current. (Song, J.-H., 2004) uses modification on duty cycle of PWM during commutation period in order to reduce commutation torque ripple in low speed region by technique OFF_PWM_PWM. In this technique, both switches of incoming phase and un-commutated phase are applied in the same duty cycle, in order to equalize the time of falling outgoing current with the time of rising incoming current by slow down the incoming current. Also in (Song, J.-H., 2004), there is another technique for commutation torque ripple reduction in high speed region, this technique is called PWM_ON_ON mode to slow down falling time of outgoing current.

Shi, J., 2013 presents a PWM modification for BLDC motor working with upper switches. This technique is suitable for full range speed. It applies PWM for three phase winding during commutation period with different duty cycle in order to equalize the rising time and the falling time for currents.

In (Salah, W., 2015 and 2011) there are similar techniques to the one proposed in (Song, J.-H., 2004) about the equality of the rising time and the falling time for currents in low speed region. But in high speed region, the modification of duty cycle of PWM in (Salah, 2015 and 2011) is in the incoming current not in the outgoing current, whereas in (Song, J.-H., 2004) the modification is in the outgoing current. In (Krishnan, R., 2010), torque ripple is minimized by advancing input phase voltage with an angle with respect to its inductors. In this method, the torque ripple enhancement becomes because the applied voltage is greater than back EMF during the period which has higher current magnitude.

Lu, H., 2008 introduces another modification for PWMs by pre-computing the duty cycle in the torque controller during normal period and commutation period, and then

they are applied to the switches. Computation of duty cycle depends on some variables such as torque feedback, actual back EMF and supply voltage in this method. However, modification of duty cycle does not end here, the controller also analyses the actual torque. If the feedback torque still can't follow the reference torque in spite of the computation of duty reaches 100%, another duty cycle is calculated and applied to slow down the outgoing current. The modification is stopped when outgoing current vanishes. Minimization of torque ripple is proposed in (Bharatkar, S.S**.,** 2008) by changing two-phase switching mode into three phase switching mode. That means there are three coils active by three switches during normal period and three coils are active by two switches and Freewheeling diode during commutation period, this mode is suitable for high speed only. Because of that, at low speed, 120^0 mode can be applied and at higher speed, 120^0 mode changes over to 180^0 mode (Bharatkar, S.S**.,** 2008). An approach to minimize torque ripple in BLDC motors is presented in (Park, S. J., 2000) by obtaining optimal excitation for the currents based on the *d-q-0* reference. These currents will be used as reference values for controller in order to force the actual currents to track them. There is another technique to reduce torque ripple in BLDC motor which is mentioned in (Berendsen, C-S., 1993). It is proposed to compensate the neutral voltage v_{n_0} in torque controller because the neutral voltage has different value during normal period and commutation period, which is reflected on the currents' value and waveforms. Also there is a significant factor which has a major role in torque ripple, it is back EMF. This factor is discussed and a method is implemented to reduce torque ripple which is caused by un-ideal back EMF in (Berendsen, C-S., 1993), by adding a predictive term to controller to compensate the limited bandwidth of current controller. Torque ripple is minimized in (Le-Huy, H., 1986) by a limited number of current harmonics that can be injected to eliminate undesirable torque harmonic selectively.

In this thesis, a controller has been suggested and implemented through numerical simulation in order to decrease commutation torque ripple. Conventional dead-beat current controller which controls the main reference voltage is used in conjunction with P-Type iterative learning controller as in Figure 2.1. During normal period, conventional dead-beat current controller is used to generate the control voltage to PWM controller whereas during commutation period, the two controllers are applied to

generate the voltage signal. In this work, there is four duty cycle of PWM has been computed in order to attenuate torque ripple. The proposed controller is performed in the current control loop. The effectiveness of both controllers have evaluated individually and collectively through simulations. The Simulation results have reflected the improvement in suppressing ripples by using P-Type ILC which anticipates and compensates an additional signal.

Figure 2.1: Proposed controller

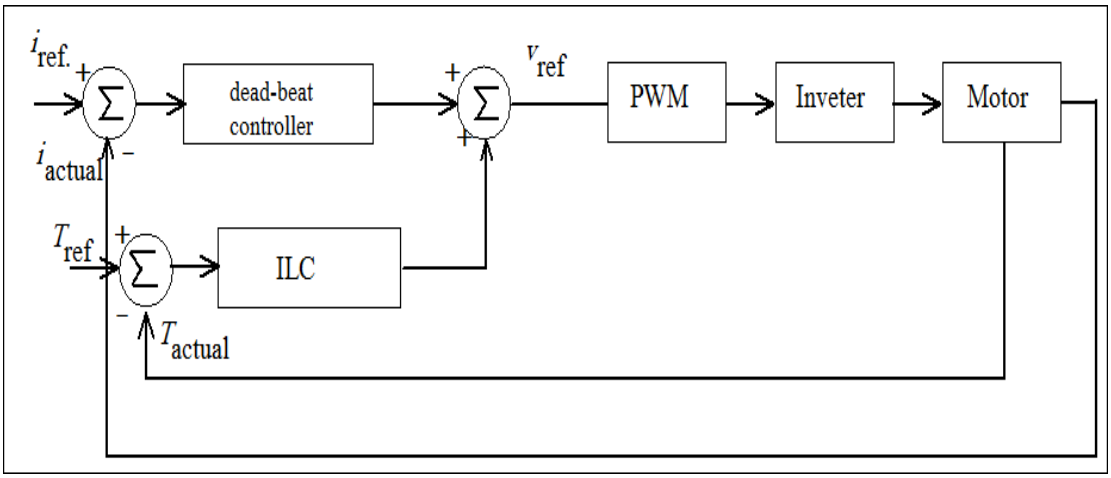

3. MODELING AND MATHEMATICAL EQUATIONS

3.1 MODELING OF BRUSHLESS DC MOTORS

The stator windings of BLDC motor consist of three coils and each coil can be represented by *R*, *L* and e where *R* is the resistance, *L* is the inductance of the winding and e refers to induced electromotive force (EMF) in the winding according to rotor spinning. By applying Kirchhoff's Voltage Law (KVL), each phase voltage can be represented by the Equations 3.1, 3.2 and 3.3 with assumptions the mutual inductance for each winding is zero, *R* and *L* are equal for all three phase and the neutral motor voltage is neglected. The equivalent circuit of BLDC motor will be in Figure 3.1.

Figure 3.1: Equivalent circuit of BLDC motor

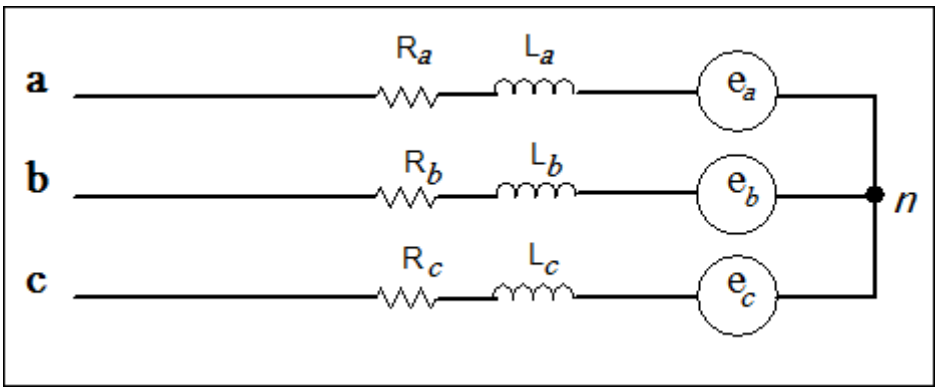

$$v_a = R * i_a + L * \frac{di_a}{dt} + e_a \quad \textbf{(3.1)}$$

$$v_b = R * i_b + L * \frac{di_b}{dt} + e_b \quad \textbf{(3.2)}$$

$$v_c = R * i_c + L * \frac{di_c}{dt} + e_c \quad \textbf{(3.3)}$$

i_a , i_b , i_c are the phase currents of motors. *R* and *L* are the resistance and inductance per phase. v_a, v_b, v_c are the phase voltages and e_a, e_b, e_c are induced back EMF in stator windings for phases a, b and c respectively. These equations describe the electrical dynamics of BLDC motor.

The mechanical dynamics equation of BLDC motor can be represented by Equation 3.5.

$$\omega = \frac{d\theta}{dt} \quad \textbf{(3.4)}$$

$$J * d\omega/dt = T_e - B * \omega - T_L \quad \textbf{(3.5)}$$

where T_e is torque which is produced by electrical power and it can be called output torque that is applied to the shaft of motor. This torque will produce mechanical power for rotating (J inertia) and overcoming the friction (B). T_L is the load torque θ , J and ω are angle of rotor position, moment of inertia and angular velocity respectively. The torque in conventional DC motor and brushless DC motor is proportional to the current in armature winding and the current in stator winding respectively as shown in Equation 3.6, and the back EMF which is generated in stator winding will depend on the angular velocity of the rotor and it is represented by Equation 3.7, by arrangement them with Equation 3.5 the molding and equations of single phase brushless DC motor can be obtained by Equations 3.9 and 3.11. Where k_e is the back EMF constant and k_t is the torque constant.

$$T_e = k_t * i \quad \textbf{(3.6)}$$

$$e = k_e * \omega \quad \textbf{(3.7)}$$

$$\frac{d\omega}{dt} = \frac{1}{J} * [T_e - B * \omega - T_L] \quad \textbf{(3.8)}$$

$$\frac{d\omega}{dt} = \frac{1}{J} * [k_t * i - B * \omega - T_L] \quad \textbf{(3.9)}$$

$$v = i * R + L * di/dt + e \quad \textbf{(3.10)}$$

$$\frac{di}{dt} = \frac{1}{L} * [v - i * R - k_e * \omega] \quad \textbf{(3.11)}$$

For BLDC motor, the electromagnetic torque in terms of back EMF can be defined as in Equation 3.12.

$$T_e = (e_a * i_a + e_b * i_b + e_c * i_c) / \omega \quad \textbf{(3.12)}$$

The instantaneous generated back EMF for each coil in stator winding can be expressed as in Equations3.13, 3.14 and 3.15.

$$e_a = k_e * f_a(\theta) * P * \omega/2 \quad \textbf{(3.13)}$$

$$e_b = k_e * f_b(\theta) * P * \omega/2 \quad \textbf{(3.14)}$$

$$e_c = k_e * f_c(\theta) * P * \omega/2 \quad \textbf{(3.15)}$$

where f_a , f_b, f_c have the same shape of e_a, e_b , e_c, but the maximum magnitude ∓ 1 (Krishnan, R.,2010) and P is the total number of stator poles. Therefore, the equation of electromagnetic torque can be given by:

$$T_e = k_e * P * \omega * \frac{f_a(\theta) * i_a + f_b(\theta) * i_b + f_c(\theta) * i_c}{2 * \omega} \quad \textbf{(3.16)}$$

3.2 INVERTER

The power supply (inverter) has 6 switches that can be MOSFETs, IGBTs or simple bipolar transistors. There are also 6 anti-parallel Freewheeling diodes (Padmaraja, Y., 2003). The thyristors are not used as switches for BLDC motor because they need time to be off after cutting PWMs' signal because its leakage currents. The switches are arranged with 3 lags while each lag has 2 switches. The three at the top are connected to positive supply voltage and the three that at the bottom to negative supply voltage as in Figure 3.2.

Figurer 3.2: Inverter and equivalent circuit for BLDC motor

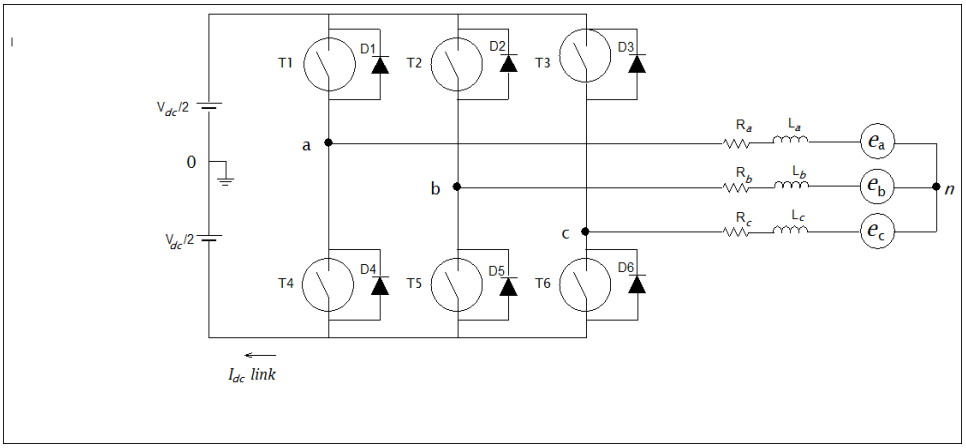

Source: Carlson, R., 1992

3.3 SECTORS

Let the sequence of energizing stator windings with supply voltage (commutation) is this sequence (ab, ac, bc, ba, ca, cb). When supply voltage is changed from a coil to another, it will be connected to all stator windings (coil a, coil b and coil c) by two switches and one freewheeling diode due to the energy stored in inductance of stator windings. This connection will be changed when freewheeling diode becomes in reverse bias at the moment of the energy stored is finished. Thus, the supply voltage will be connected to two coils by the two switches. This situation is repeated six times due to the 6 commutation in one electrical cycle as in Figure 3.3 and each one of them is called sector. From analysis the waveforms, the details of sectors will be given in Table 3.1. Considering the previous sequence is forward direction rotation, the reverse direction will be (ac, ab, cb, ca, ba, bc).

Figure 3.3: Sectors' waveforms (Voltages and currents)

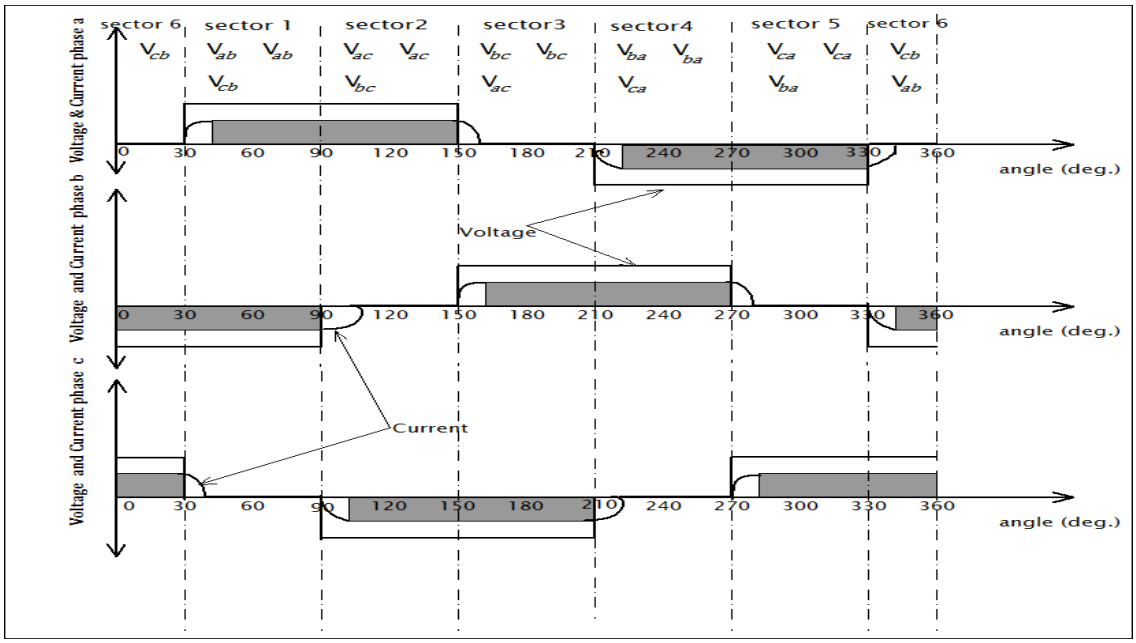

Source: Krishnan, R., 2010

Table 3.1: Sectors voltage table

Sector	Angle	v_{a_0}	v_{b_0}	v_{c_0}	Phases' connect.	Phases' connect.
Sector 1	$30^0 < \theta_e <= 90^0$	$v_{a=+}$	$v_{b=-}$	$v_{c=-}$ until $i_c = 0$	v_{ab} v_{cb}	v_{ab} If $i_c = 0$
Sector 2	$90^0 < \theta_e <= 150^0$	$v_{a=+}$	$v_{b=+}$ until $i_b = 0$	$v_{c=-}$	v_{ac} v_{bc}	v_{ac} If $i_b = 0$
Sector 3	$150^0 < \theta_e < = 210^0$	$v_{a=-}$ until $i_a = 0$	$v_{b=+}$	$v_{c=-}$	v_{bc} v_{ac}	v_{bc} If $i_a = 0$
Sector 4	$210^0 < \theta_e <= 270^0$	$v_{a=-}$	$v_{b=+}$	$v_{c=+}$ until $i_c = 0$	v_{ba} v_{ca}	v_{ba} If $i_c = 0$
Sector 5	$270^0 < \theta_e <= 330^0$	$v_{a=-}$	$v_{b=-}$ until $i_b = 0$	$v_{c=+}$	v_{ca} v_{ba}	v_{ca} If $i_b = 0$
Sector 6	$330^0 < \theta_e <= 30^0$	$v_{a=+}$ until $i_a = 0$	$v_{b=-}$	$v_{c=+}$	v_{cb} v_{ab}	v_{cb} If $i_a = 0$

Let's discuss and analyse commutation from (cb) to (ab). After switching positive supply voltage from coil c to coil a, coil c will be connected to negative supply voltage by freewheeling diode due to the energy stored in its inductance. The equivalent circuit of BLDC motor will be as in Figure 3.4 by assuming v_a, v_b and v_c are v_1, v_2 and v_3 respectively. In this circuit, there are currents in two electrical meshes. Dynamics of these currents can be determined by Kirchhoff's Voltage Law (KVL). The value of the sum of BLDC's phase currents at any time is zero as in Equation 3.17 and the neutral voltage (v_{n_0}) is neglected.

Figure 3.4: General equivalent circuit during commutation

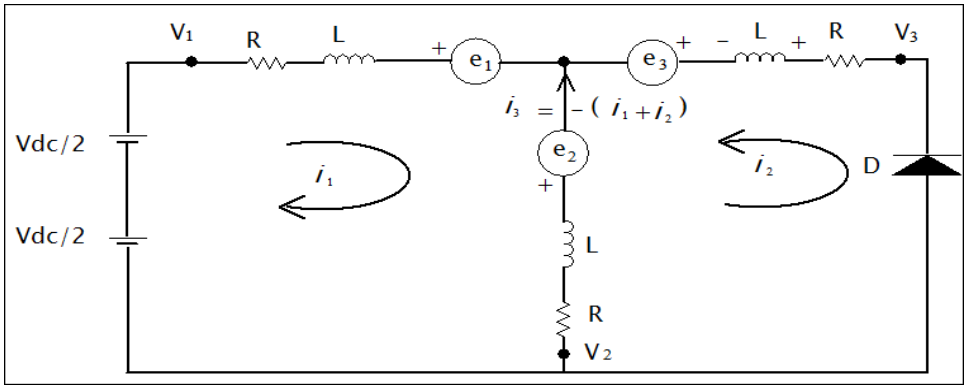

$$i_1 + i_2 + i_3 = 0 \qquad \textbf{(3.17)}$$

Applying KVL for mesh 1:

$$V_1 - R * i_1 - L * \frac{di_1}{dt} - \mathrm{e}_1 + \mathrm{e}_2 - R * i_1 - L * \frac{di_1}{dt} - V_2 - R * i_2 - L * \frac{di_2}{dt} = 0 \qquad \textbf{(3.18)}$$

Applying KVL for mesh 2:

$$V_3 - R * i_2 - L * \frac{di_2}{dt} - \mathrm{e}_3 + \mathrm{e}_2 - R * i_2 - L * \frac{di_2}{dt} - V_2 - R * i_1 - L * \frac{di_1}{dt} = 0 \qquad \textbf{(3.19)}$$

Placing the derivatives on one side:

$$2 * L * \frac{di_1}{dt} + L * \frac{di_2}{dt} = -2 * R * i_1 - R * i_2 + V_1 - V_2 - \mathrm{e}_1 + \mathrm{e}_2 \qquad \textbf{(3.20)}$$

$$L * \frac{di_1}{dt} + 2 * L * \frac{di_2}{dt} = -R * i_1 - 2 * R * i_2 + V_3 - V_2 - \mathrm{e}_3 + \mathrm{e}_2 \qquad \textbf{(3.21)}$$

Multiply Equation 3.20 by 2 and Equation 3.21 by -1 and combine them:

$$3 * L * \frac{di_1}{dt} = -3 * R * i_1 + 2 * V_1 - V_2 - V_3 - 2 * \mathrm{e}_1 + \mathrm{e}_2 + \mathrm{e}_3 \qquad \textbf{(3.22)}$$

Finally, multiply Equation 3.20 by 1, Equation 3.21 by -2 and combine them:

$$-3 * L * \frac{di_2}{dt} = 3* R * i_2 - 2 * V_3 + V_2 + V_1 + 2 * e_3 - e_1 - e_2 \quad \textbf{(3.23)}$$

Thus,

$$\frac{di_1}{dt} = \frac{1}{3*L} * [-3* R * i_1 + 2 * V_1 - V_2 - V_3 - 2 * e_1 + e_2 + e_3] \quad \textbf{(3.24)}$$

$$\frac{di_2}{dt} = \frac{1}{3*L} * [-3* R * i_2 + 2 * V_3 - V_1 - V_2 - 2 * e_3 + e_1 + e_2] \quad \textbf{(3.25)}$$

Also from Equation3.17,

$$\frac{di_3}{dt} = -(\frac{di_1}{dt} + \frac{di_2}{dt}) \quad \textbf{(3.26)}$$

can be resulted. Equations3.24, 3.25 and 3.26 are the general differential equations for all sectors during commutation period until the current of coil which is separated from supply voltage is equal zero. The value of these equations is depended on the supply voltage (PWM), previous coil connections with supply voltage and the back EMF. When the freewheeling diode becomes in reverse bias, the current derivatives equations are presented by:

$$\frac{di_1}{dt} = \frac{1}{L} * [V_1 - R * i_1 - e_1] \quad \textbf{(3.27)}$$

$$\frac{di_3}{dt} = \frac{1}{L} * [V_2 - R * i_3 - e_2] \quad \textbf{(3.28)}$$

From the above analysis, the current derivatives equations for each sector in Figure 3.3 can be calculated:

1. Sector 1: $30^0 < \theta_e <= 90^0$

Commutation from sector 6 (cb) to sector 1 (ab), when $i_c > 0$, the current derivatives equations during commutation period are presented by:

$$\frac{di_a}{dt} = \frac{1}{3*L} * [-3* R * i_a + 2 * V_a - V_b - V_c - 2 * e_a + e_b + e_c] \quad \textbf{(3.29)}$$

$$\frac{di_c}{dt} = \frac{1}{3*L} * [-3* R * i_c + 2 * V_c - V_a - V_b - 2 * e_c + e_b + e_a] \quad \textbf{(3.30)}$$

$$\frac{di_b}{dt} = -\left(\frac{di_a}{dt} + \frac{di_c}{dt}\right) \quad \textbf{(3.31)}$$

If i_c reaches to zero, the current derivatives are given below:

$$\frac{di_a}{dt} = \frac{1}{L} * [\, V_a - R * i_a - \mathrm{e}_a] \quad \textbf{(3.32)}$$

$$\frac{di_b}{dt} = \frac{1}{L} * [\, V_b - R * i_b - \mathrm{e}_b] \quad \textbf{(3.33)}$$

2. Sector 2: $90^0 < \theta_e <= 150^0$

Commutation from sector 1 (ab) to sector 2 (ac), when $i_b < 0$, the current derivatives equations during commutation period are presented by:

$$\frac{di_a}{dt} = \frac{1}{3*L} * [\, -3* R * i_a + 2 * V_a - V_a - V_b - 2 * \mathrm{e}_a + \mathrm{e}_b + \mathrm{e}_c] \quad \textbf{(3.34)}$$

$$\frac{di_b}{dt} = \frac{1}{3*L} * [\, -3* R * i_b + 2 * V_b - V_a - V_c - 2 * \mathrm{e}_b + \mathrm{e}_a + \mathrm{e}_c] \quad \textbf{(3.35)}$$

$$\frac{di_c}{dt} = -\left(\frac{di_b}{dt} + \frac{di_a}{dt}\right) \quad \textbf{(3.36)}$$

If i_b reaches to zero, the current derivatives are given below:

$$\frac{di_a}{dt} = \frac{1}{L} * [\, V_a - R * i_a - \mathrm{e}_a] \quad \textbf{(3.37)}$$

$$\frac{di_c}{dt} = \frac{1}{L} * [\, V_c - R * i_c - \mathrm{e}_c] \quad \textbf{(3.38)}$$

3. Sector 3: $150^0 < \theta_e <= 210^0$

Commutation from sector 2 (ac) to sector 3(bc) when $i_a > 0$, the current derivatives equations during commutation period are presented by:

$$\frac{di_b}{dt} = \frac{1}{3*L} * [\, -3* R * i_b + 2 * V_b - V_a - V_c - 2 * \mathrm{e}_b + \mathrm{e}_a + \mathrm{e}_c] \quad \textbf{(3.39)}$$

$$\frac{di_a}{dt} = \frac{1}{3*L} * [\, -3* R * i_a + 2 * V_a - V_b - V_c - 2 * \mathrm{e}_a + \mathrm{e}_b + \mathrm{e}_c] \quad \textbf{(3.40)}$$

$$\frac{di_c}{dt} = -\left(\frac{di_b}{dt} + \frac{di_a}{dt}\right) \quad \textbf{(3.41)}$$

If i_a reaches to zero, the current derivatives are given below:

$$\frac{di_b}{dt} = \frac{1}{L} * [\, V_b - R * i_b - \mathrm{e}_b] \quad \textbf{(3.42)}$$

$$\frac{di_c}{dt} = \frac{1}{L} * [\, V_c - R * i_c - \mathrm{e}_c] \quad \textbf{(3.43)}$$

4. Sector 4: $210^0 < \theta_e <= 270^0$

Commutation from sector 3 (bc) to sector 4 (ba) when $i_c < 0$, the current derivatives equations during commutation period are presented by:

$$\frac{di_b}{dt} = \frac{1}{3*L} * [\, -3* R * i_b + 2 * V_b - V_a - V_c - 2 * \mathrm{e}_b + \mathrm{e}_a + \mathrm{e}_c] \quad \textbf{(3.44)}$$

$$\frac{di_c}{dt} = \frac{1}{3*L} * [\, -3* R * i_c + 2 * V_c - V_a - V_b - 2 * \mathrm{e}_c + \mathrm{e}_b + \mathrm{e}_a] \quad \textbf{(3.45)}$$

$$\frac{di_b}{dt} = -\left(\frac{di_c}{dt} + \frac{di_a}{dt}\right) \quad \textbf{(3.46)}$$

If i_c reaches to zero, the current derivatives are given below:

$$\frac{di_b}{dt} = \frac{1}{L} * [\, V_b - R * i_b - \mathrm{e}_b] \quad \textbf{(3.47)}$$

$$\frac{di_a}{dt} = \frac{1}{L} * [\, V_a - R * i_a - \mathrm{e}_a] \quad \textbf{(3.48)}$$

5. Sector 5: $270^0 < \theta_e <= 330^0$

Commutation from sector 4 (ba) to sector 5 (ca) when $i_b > 0$, the current derivatives equations during commutation period are presented by:

$$\frac{di_c}{dt} = \frac{1}{3*L} * [\, -3* R * i_c + 2 * V_c - V_a - V_b - 2 * \mathrm{e}_c + \mathrm{e}_b + \mathrm{e}_a] \quad \textbf{(3.49)}$$

$$\frac{di_b}{dt} = \frac{1}{3*L} * [\, -3* R * i_b + 2 * V_b - V_a - V_c - 2 * \mathrm{e}_b + \mathrm{e}_a + \mathrm{e}_c] \quad \textbf{(3.50)}$$

$$\frac{di_a}{dt} = -\left(\frac{di_b}{dt} + \frac{di_c}{dt}\right) \quad \textbf{(3.51)}$$

If i_b reaches to zero, the current derivatives are given below:

$$\frac{di_c}{dt} = \frac{1}{L} * [\, V_c - R * i_c - \mathrm{e}_c] \quad \textbf{(3.52)}$$

$$\frac{di_a}{dt} = \frac{1}{L} * [\, V_a - R * i_a - \mathrm{e}_a] \quad \textbf{(3.53)}$$

6. Sector 6: $330^0 < \theta_e <= 30^0$

Commutation from sector 5 (ca) to sector 6 (cb) when $i_a < 0$, the current derivatives equations during commutation period are presented by:-

$$\frac{di_c}{dt} = \frac{1}{3*L} * [\, -3* R * i_c + 2 * V_c - V_a - V_c - 2 * \mathrm{e}_c + \mathrm{e}_a + \mathrm{e}_b] \quad \textbf{(3.54)}$$

$$\frac{di_a}{dt} = \frac{1}{3*L} * [\, -3* R * i_a + 2 * V_a - V_b - V_c - 2 * \mathrm{e}_a + \mathrm{e}_b + \mathrm{e}_c] \quad \textbf{(3.55)}$$

$$\frac{di_c}{dt} = -\left(\frac{di_b}{dt} + \frac{di_a}{dt}\right) \quad \textbf{(3.56)}$$

If i_a reaches to zero, the current derivatives are given below:

$$\frac{di_c}{dt} = \frac{1}{L} * [\, V_c - R * i_c - \mathrm{e}_c] \quad \textbf{(3.57)}$$

$$\frac{di_b}{dt} = \frac{1}{L} * [\, V_b - R * i_b - \mathrm{e}_b] \quad \textbf{(3.58)}$$

3.4 WAVEFORMS OF HALL EFFECT SENSORS

Knowing rotor position is very important for controller to determine which coil should be energized. In some motors, there are three hall effect sensors sense rotor position. Hall sensors will generate voltage signals when the north pole passes near of sensors and this voltage will stay at high level until the south pole passes near to the same sensor. When rotor consists of two poles and the angle between sensors is 120^0 the signal of sensor will stay high for 180^0 until the south pole passes near the same sensor which was the north pole had been passed near it in first. And the second sensor will generate voltage after the sensor 1 with phase shifting is 120°. Similarly, the third sensor will generate high level voltage after sensor 2 with phase shifting is 120° and 240° with respect to sensor 2 and 1 respectively. Figure 3.5 depicts the waveforms of Hall Effect sensors in motor has rotor with only two poles.

Figure 3.5: Hall effect sensors' waveforms for rotor 2 pole

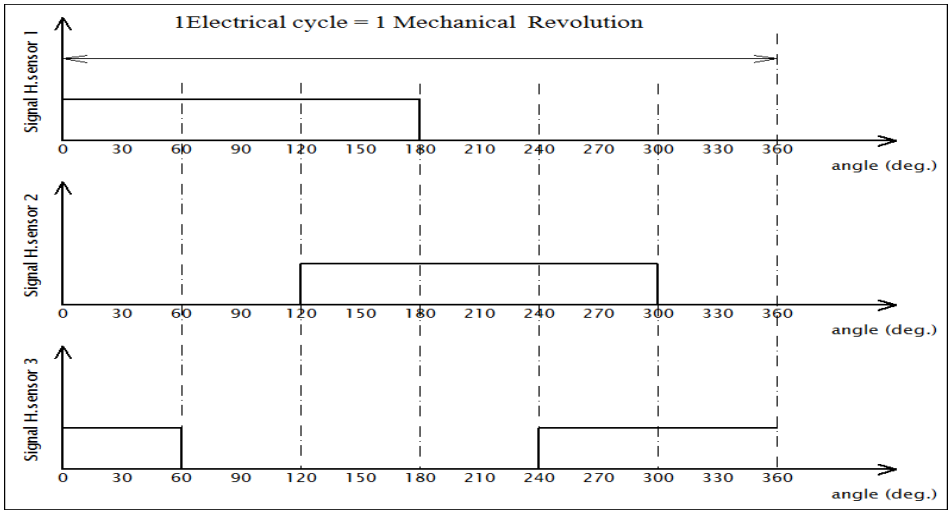

Source: Brown, W., 2002

In Figure 3.5, the high level voltage produced from hall effect sensors is equal to 1 and the low level voltage is equal to 0, then, the truth table of all waveforms were generated from sensors of rotor has 2 poles is given in Table 3.2. From the table, it is clear that the controller will receive only six situations every 360^0 and it will never see 000, 111.

Table 3.2: Truth table for hall effect sensors, rotor 2 pole

Hall sensor1	Hall sensor2	Hall sensor3	Rotor Angle
1	0	1	$0^0 < \theta_e <= 60^0$
1	0	0	$60^0 < \theta_e <= 120^0$
1	1	0	$120^0 < \theta_e <= 180^0$
0	1	0	$180^0 < \theta_e <= 240^0$
0	1	1	$240^0 < \theta_e <= 300^0$
0	0	1	$300^0 < \theta_e <= 360^0$

3.5 ELECTROMOTIVE FORCE BACK (EMF)

According to Lenz's law, when the electrical current passes through a winding which intersects the magnetic field, electro motive force is generated in this winding. Similarly this voltage can be generated in BLDC motors when the permanent magnet rotor spins and its constant magnetic field intersects the stator winding which was energized with

DC supply voltage. As a result of that, voltage is induced in each winding which opposes the supply voltage in polarity and this voltage is known as back EMF The magnitude of this voltage depends on (Padmaraja, Y., 2003).:

1. *"Rotor's angular velocity.*
2. *Number of turns in each stator winding.*
3. *Magnetic field generated by rotor".*

This voltage is depended on some factors as in Equation 3.59:

$$Back\ EMF = NlrB\omega \quad \textbf{(3.59)}$$

Where N is the number of winding turns per phase, l is the length of the rotor, r is the internal radius of the rotor, B is the rotor magnetic field density and ω is the rotor's angular velocity.

Once a motor is produced, the number of turns in stator winding and the magnetic field generated by the rotor takes constant values depending on the manufacturing process. Therefore the rotor's angular velocity is the only variable manipulating the magnitude of the back EMF as in Equation 3.60.

$$\mathrm{e} = k_e * \omega \quad \textbf{(3.60)}$$

where e is back EMF, k_e is back EMF constant and ω is the rotor's angular velocity. In brushless DC motors, the waveforms of back EMF signals are trapezoidal and symmetrical across axis with 120^0 phase shift between them in ideal conditions. Under these conditions, the currents of stator windings are desired to have rectangular shapes as shown in Figure 3.6. Consequently, the torque produced by the motor becomes smooth without ripple. But, in fact, the waveforms of back EMFs are neither symmetrical nor trapezoidal in practice and the shift angle between them is not equal to 120^0 either. This situation leads to torque pulsation and ripples. In addition, back EMF depends on angular velocity of the rotor and it will not be generated when the motor is stationary or in very low speed. Therefore it is difficult to measure these signals and that may reflect on the design of some controllers, especially the controllers are depended on back EMF in its structure. The voltage on each stator winding can be calculated

mathematically by Kirchhoff's voltage law (KVL). The potential difference between DC bus voltage and the back EMF will cause the motor to give rated current and to produce rated torque. When back EMF is equal to supply voltage the current and torque will both equal zero and when it is high, the potential across winding will be decrease that means the current and torque will be low (Keeping, S., 2014).

Figure 3.6: Ideal back EMF's and rectangular currents

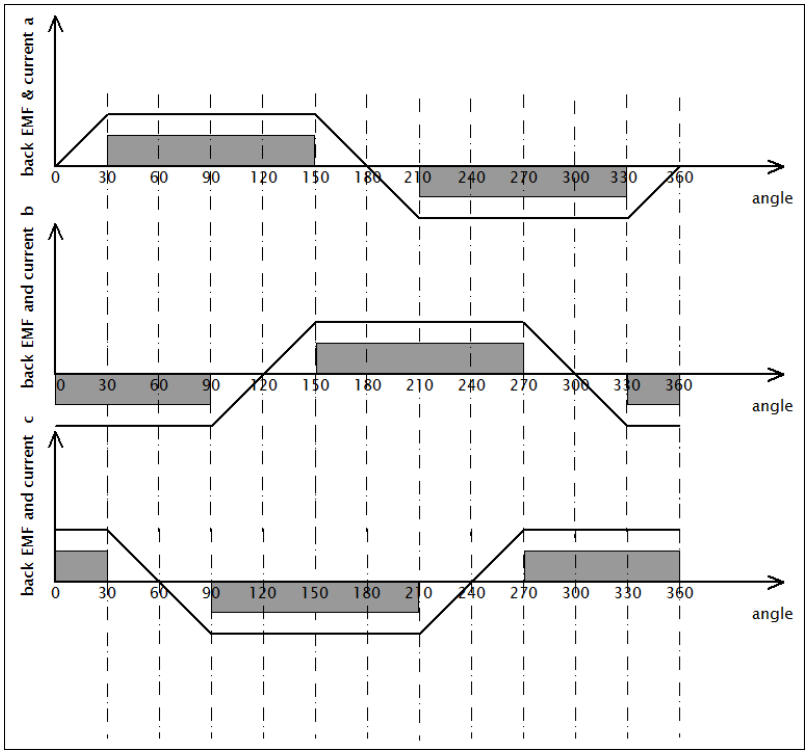

Source: Lin, H., 2009

3.6 TORQUE RIPPLE

3.6.1 DEFINITION AND CAUSES

Torque ripple is an effect that can be seen in motor applications, which indicates a periodic variation in the output torque as the motor shaft rotates. It is usually measured as maximum torque minus minimum torque over one complete revolution, and generally expressed as percentage (Anand, K., 2014) as in Equation 3.61.

$$\text{Amount of torque ripple} = [\, T_{MAX} - T_{MIN} \,] / T_{AVEARAGE} * 100\ \% \qquad \textbf{(3.61)}$$

There are several types of torque ripple and several reasons for those (Salah, W. 2011):

1. Motor structure: *A. Air gap.*

B. Flux linkage.

C. Non trapezoidal back (EMF).

2. Motor nature: *A. Cogging torque.*

B. Reluctance torque.

C. Electromagnetic torque.

3. Motor control: *A. PWM scheme.*

B. Current commutation 1. Power supply inverter.

2. Current commutation.

3. Freewheeling Diode.

Existence of ripples in torque leads to vibration, noise, speed ripples and fluctuations thereby defects and deviates the applications. Moreover, torque ripple is the one major reason restricting the usage of BLDC motors in application requiring higher performance.

Once a motor has been produced and implemented in an application, the ripple produced by motor's nature and structure is constant and depending on the manufacturing process. Because of that, it is difficult to eliminate these kinds of ripples by a controller. Therefore the ripple is produced by motor control is easier to attenuate than the others. This ripple can be classified in two parts: the first one is the switching torque ripple and the second one is a commutation torque ripple.

The switching torque ripple is smaller, has high frequency and averaging less than commutation torque ripple because it is produced by pulse width modulation itself (PWM) with frequency may reach to 20 KHZ. This ripple occurs when PWM is applied on two switches to connect stator windings with supply voltage (Shi, J., 2013). The commutation torque ripple is produced when switching supply voltage or current from coil to coil. This torque is stronger and sudden (Shi, J., 2013).

3.6.2 COMMUTATION TORQUE RIPPLE

BLDC motor consists of three main parts; the stator winding, permanent magnetic rotor and the hall effect sensors. Interaction between the magnetic fields generated by stator windings and the magnetic field generated by the permanent magnet rotor rotate the rotor. This rotation generates electric voltage in the stator windings according to Lenz's law. From the structure and design of the BLDC motor, these induced voltages in stator windings are trapezoidal and the currents are rectangular in ideal conditions. Due to these ideal conditions, the torque can be generated free from ripple (spikes or dips) except commutation. In fact there is ripple in torque due to the reasons that mentioned earlier in Section 3.6.1 and because there is not ideal conditions in nature. In order to eliminate the ripple one should know how it is generated. In case of usage hall effect sensors, there are three hall effect sensors are placed in motor with difference angle between them 120°. These sensors produce signals for controller in order to determine which coils should be connected to supply. These sensors update its position every 60° during one electrical cycle (360°). This update is necessary to make rotation in regular and get maximum torque by making the rotor trying to catch up with magnetic field of stator winding regularly. The latest field is in advance of the rotor magnetic field with angle of 90° in ideal situation but in reality the angle varies from 60° to 120° (Berendsen ,C-S., 1993). The updating process of sensors' signals makes the inverter updates its situation 6 times through one electrical cycle of 360°. During one electrical cycle there are 6 sectors of commutation between switches. Each sector is divided into two unequal parts; the first one is called normal conduction period and the second part is called commutation period. In normal period, one of the coils is connected to positive voltage and another coil is connected to negative voltage, whereas the third one will be open. In this case, the motor control ripples arising from PWM and imperfect back EMF signals.

3.6.3 ANALYSIS OF COMMUTATION TORQUE RIPPLE

Due to the inductance in winding the energy is stored temporally in coils and according to Lenz's law the energy makes each coil a voltage source which opposes the current that caused it.

In commutation period, when the voltage supply is turned on from one coil to another, the three coils are connected to the supply voltage one of them is connected to positive voltage and the other to negative voltage whereas the third is either to positive or negative voltage depending on its storing energy and previous connection. The connection for the third coil will be by freewheeling diode. This period, is the most important part of the presence a ripple in torque and the most important part for controller is to reduce. For example, as in Figure 3.7, the coils a and c are connected to positive and negative supply by T1, T6 respectively. Then, when the commutation period begins, T1 is switched off while T2 is switched on which changes the phase connection from (ac) to (bc) as in Figure 3.8. In this period the coil a is separated from supply by cutting the PWM on T1. But in fact, phase a will be connected to negative supply by freewheeling diode D4 which is anti-parallel with T4 as in Figure 3.9 because of the energy which was stored in its inductance. This situation leads that the three phases become active during commutation period, and because of that the waveforms of phase currents would be affected. This effect appears evidently in the current of coil which is not directly involved in the process of commutation (Carlson, R., 1992). Consequently either spikes or dips will appear in this current and this is reflected on the torque by appearing the ripple. It is worth mentioning that this period should be short as much as possible in order to reduce the ripple in commutation period.

Figure 3.7: Normal period before commutation (2 coils active)

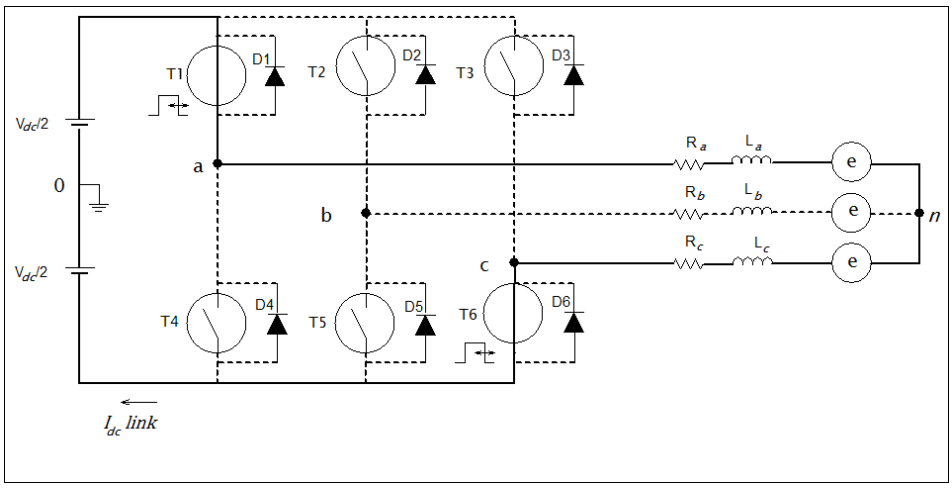

Source: Carlson, R., 1992

Figure 3.8: After end of commutation (2 coils active)

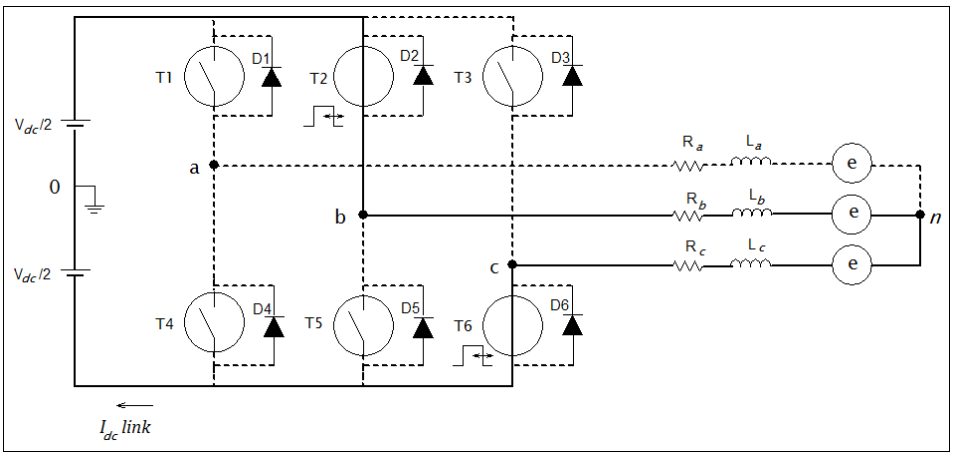

Source: Carlson, R., 1992

Figure 3.9: During commutation (3 coils active)

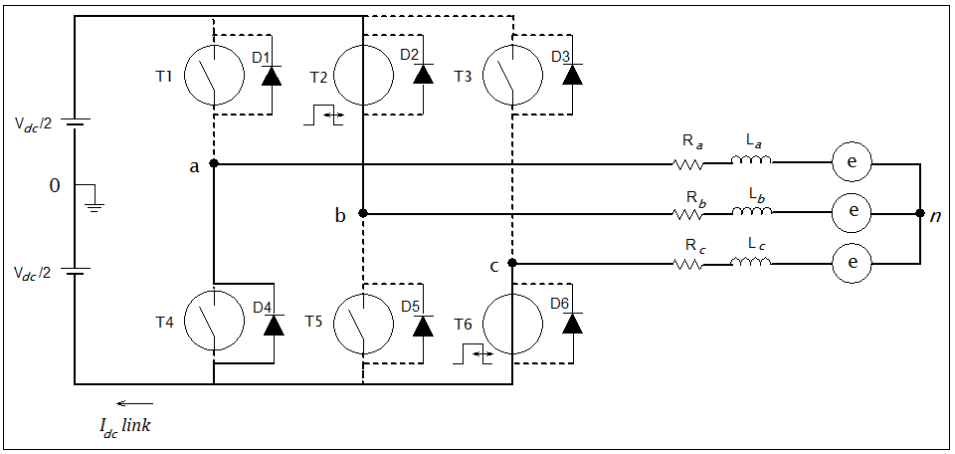

Source: (Carlson, R., 1992).

There are three definitions of currents in commutation period. The current of coil which is separated from supply is called outgoing current. the current of coil which is connected to supply instead of the outgoing phase is called the incoming current, and the current of the third coil which stays connected to supply is called un-commutated current (Lu, H., 2008), (Berendsen, C-S., 1993). In commutation period, outgoing current needs some time to vanish due to the storing energy in its inductance and the incoming current needs some time to reach to its steady-state value due to its inductance. According to above analysis, there are cases for currents' behavior that are started with switching from coil to coil (Carlson, R., 1992):

Case 1:

The outgoing current reaches to zero at same time with incoming current reaches to steady state value as in Figure 3.10. In this case the un-commutated current and torque are not affected and the sequence of transitions will be from Figure 3.7 to Figure 3.9 to Figure 3.8.

Figure 3.10: Currents' waveforms in case 1

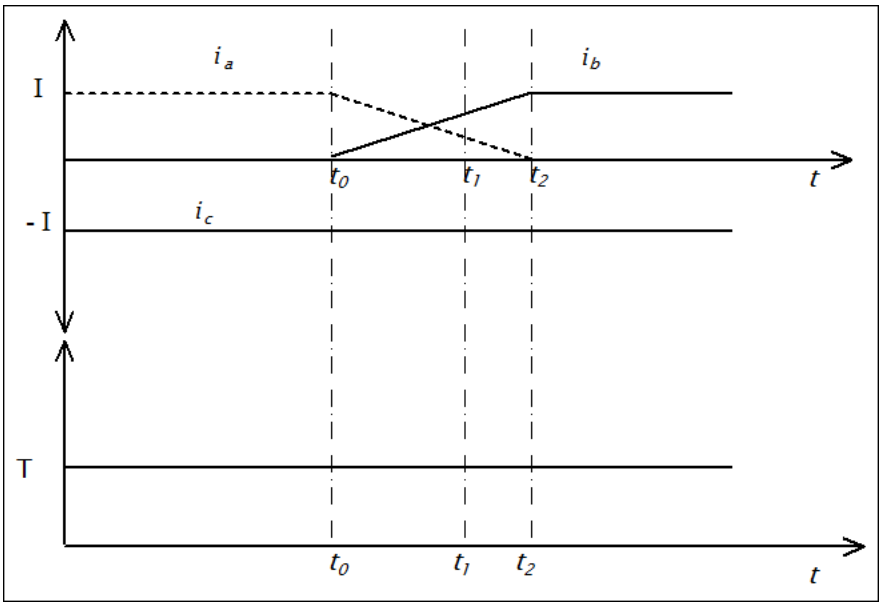

Source: Carlson, R., 1992

Case 2

In this case, outgoing current is faster than incoming current. That means, outgoing current reaches to zero before incoming current reaches to its steady-state value as in Figure 3.11. In this case the following sequence will start just after incoming current reaches to steady-state value (Carlson, R., 1992) and at this moment the commutation period is finished and the normal period for next sector is started. Before that, the un-commutated current is affected by appearing a spike in its waveform and the torque has a ripple as a dip in its waveform. Finally, the sequence of switching process will be from Figure 3.7 to 3.9 to Figure 3.8 after incoming current reaches to steady-state value.

Figure 3.11: Currents' waveforms in case 2

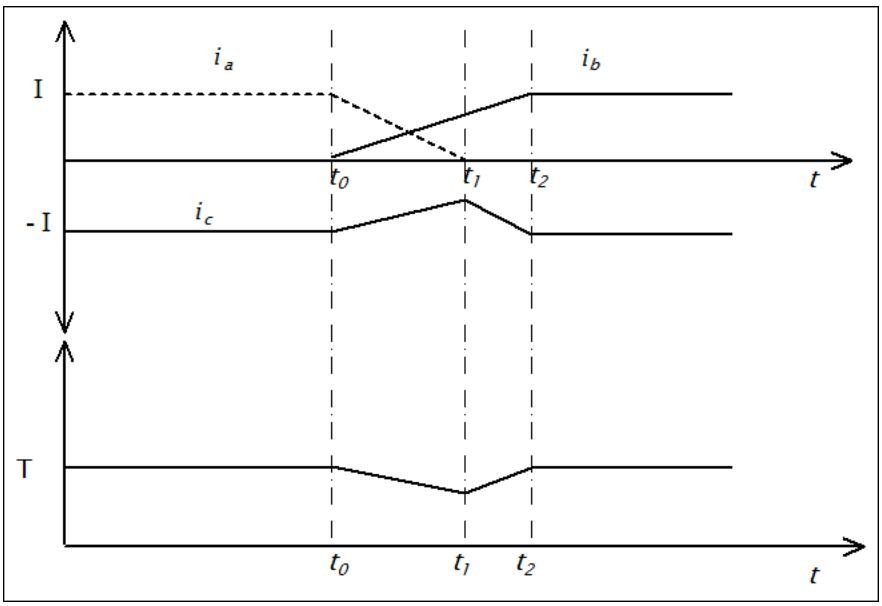

Source: Carlson, R., 1992

Case 3

Incoming current is faster than outgoing current. That means, incoming current reaches to steady-state value before outgoing current reaches to zero as shown in Figure 3.12. In this case the following sequence is different from two previous cases because the three coils of stator are connected to supply by the three anti-parallel freewheeling diodes as in Figure 3. 13. This connection stays active until outgoing current reaches to zero. At this moment the commutation period is finished and the normal period of this sector is started with two coils. Because of that connection, the dip appears in un-commutated current's waveform and the spike appears in torque. Moreover, the sequence of switching process is from Figure 3.7 to Figure 3.9 to Figure 3.13 ending in Figure 3.8.

Figure 3.12: Currents' waveforms in case 3

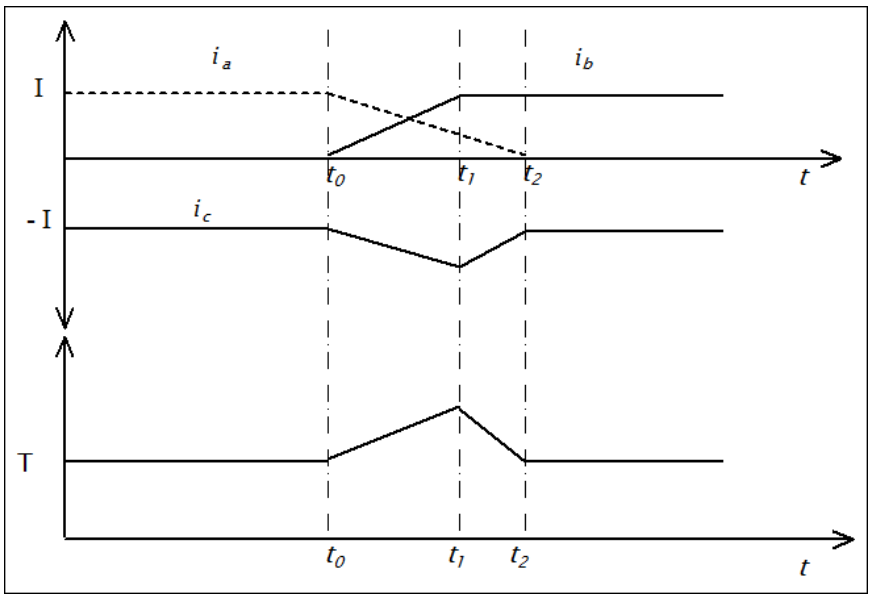

Source: Carlson, R., 1992

Figure 3.13: During commutation 3 coils active by 3 freewheeling diodes

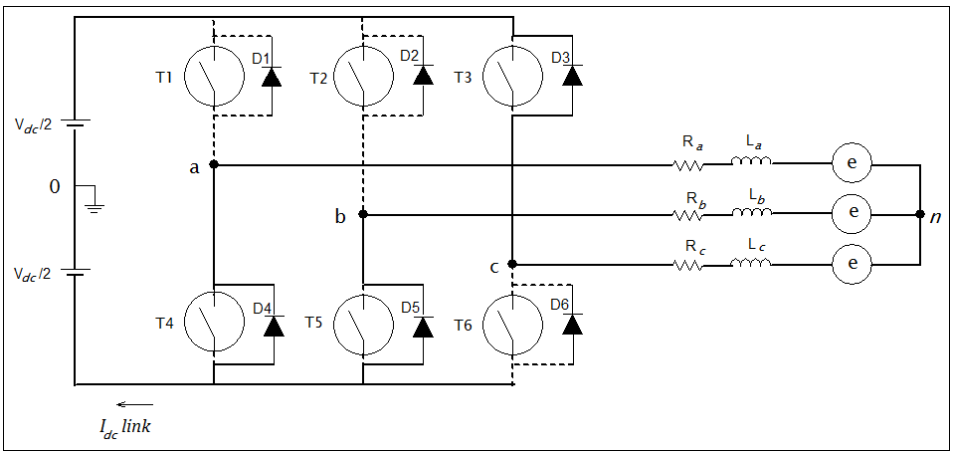

Source: Carlson, R., 1992

3.6.4 TORQUE EQUATIONS

The electromagnetic torque of BLDC motors can be defined as in Equation 3.62 (Krishnan, R., 2010).

$$T_e = (e_a * i_a + e_b * i_b + e_c * i_c) / \omega \quad \textbf{(3.62)}$$

From Equation 3.62, torque is proportional to the current and back EMF in each coil in stator winding. In order to produce regular and maximum torque, the supply voltage

should be turned from coil to coil 6 times during one electrical cycle. Let the sequence of commutation is (ab, ac, bc, ba, ca, cb) as in Figure 3.14.

Figure 3.14: Commutation during 1 electrical cycle (Currents and EMFs)

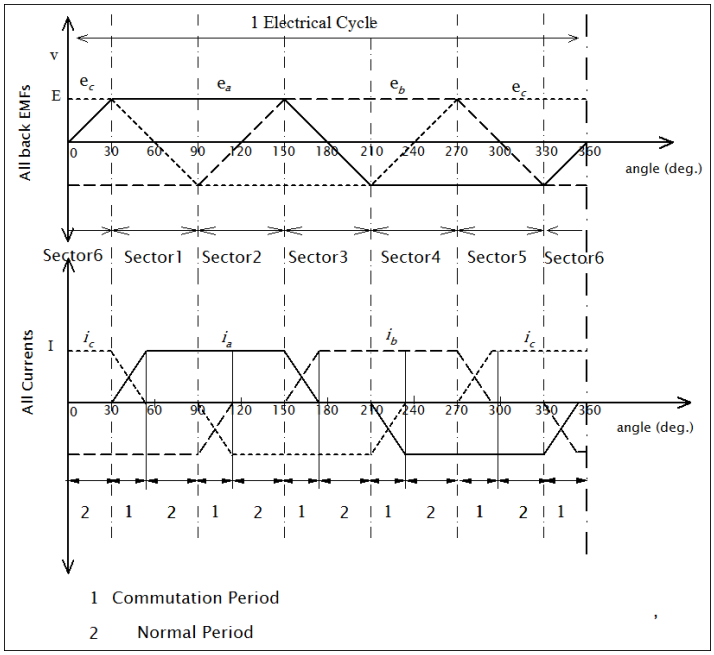

In this figure, there are 6 intervals or sectors and each one of them is divided into two periods; the first one is called commutation period and the other is called normal period. In normal period of each sector, there are two coils are active and in commutation period, there are three coils are active. Therefore, from Figure 3.14, the torque equations can be deduced in all sectors as in Table 3.3.

Table 3.3: Torque Equations in all sectors

Sector	Normal period (2 coils active)	Commutation period (3 coils active)
1	$T_e = (e_a * i_a + e_b * i_b) / \omega$	$T_e = (e_a * i_a + e_b * i_b + e_c * i_c) / \omega$
2	$T_e = (e_a * i_a + e_c * i_c) / \omega$	$T_e = (e_a * i_a + e_b * i_b + e_c * i_c) / \omega$
3	$T_e = (e_b * i_b + e_c * i_c) / \omega$	$T_e = (e_a * i_a + e_b * i_b + e_c * i_c) / \omega$
4	$T_e = (e_b * i_b + e_a * i_a) / \omega$	$T_e = (e_a * i_a + e_b * i_b + e_c * i_c) / \omega$
5	$T_e = (e_c * i_c + e_a * i_a) / \omega$	$T_e = (e_a * i_a + e_b * i_b + e_c * i_c) / \omega$
6	$T_e = (e_c * i_c + e_b * i_b) / \omega$	$T_e = (e_a * i_a + e_b * i_b + e_c * i_c) / \omega$

3.7 THE OTHER REASONS FOR THE RIPPLE

1. Most of the BLDC motors which are used in practical applications with star connection for stator windings, the voltage between neutral point of these windings and neutral point of inverter should be zero. But in fact, a difference voltage exists between them, this voltage will lead to disturbance in phases current especially in beginning of commutation and these voltage depends on the back EMF (Berendsen, C-S., 1993). Not only there is a voltage between the 2 points but also the value of it is different in normal conduction period and commutation period as in Equation 3.63 and 3.64 respectively.

$$v_{n_0} = -\frac{v_{\mathrm{dc}}}{6} - \frac{(\mathrm{e}_a+\mathrm{e}_b+\mathrm{e}_c)}{3} \quad \textbf{(3.63)}$$

$$v_{n_0} = -\frac{(\mathrm{e}_b+\mathrm{e}_c)}{2} \quad \textbf{(3.64)}$$

2. The conversion from analog signal to digital causes a torque ripple (Yuan, Y., 2011).
3. the nonlinearity of the physical devices in the inverter leads to ripple. In other words the switching characteristic for the six switches are not ideal.
4. Some mechanical deviations cause torque ripple. For example, mechanical bias and unequal distribution of friction in the bearings lead to ripple (Yuan, Y., 2011).
5. The dc offset in stator current measurements also leads to pulsating torque. The presence of any unbalanced dc supply voltage in the current sensors and inherent offsets in the analog electronic devices give rise to dc offsets (Qian, W., 2005).
6. The presence of no integer or pseudo harmonics which induced from load side in the non-ideal loading mechanism leads to ripples (Qian, W., 2005).
7. There is another reason which plays a major role in existence the ripple torque, it is un-ideal back EMF. Un-ideal back EMF will cause un-rectangular currents. That will be reflected on torque's waveforms because the output torque in BLDC motor is proportional to the currents and back EMF as in Equation 3.62.

3.8 LEARNING CONTROLLERS

Life is a school and its experiences are a key for success. Learning from events and its repetition builds success and reduces error. These arguments are possible to reflect on the design of electrical controllers where they can take advantages from the key of argument which is the repetition. Learning controllers have been used in systems that have performance in same operation repeatedly and under same operating conditions within considering the same initial starting. Even though the error signals which are known and measured from previous steps have much information that can be used, they are typically unused and ignored in non-learning systems. The using of these signals can be useful to improve the performance of control systems, which implement the same task, by learning from previous iterations. Practically the name of this controller is learning controllers and there are some types of learning controllers:

1. Iterative learning controller (ILC)
2. Repetitive controller (RC)
3. Adaptive controller (AC)
4. Neural networks controller (NN)

3.8.1 THE COMPARISON BETWEEN THE TYPES

Iterative learning controller is used for discontinuous operation and dedicated for devices which often comeback to home position when it finishes its task (initial condition). The others do not return to initial starting rather than they start from the point which they are stopped on it. This controller mainly used in industrial applications which needs home position and in the applications that regard the importance of the information which are collected from previous iterations such as computer numerical control (CNC) (Kim, D. I.,1996), industrial robots, induction motors, metal rolling (Ma, T.-T., 2009) and brushless DC motors. ILC can be used for applications which do not have identical repetition such as robots which do same tasks but they are not in same period of time. Finally, ILC modifies the control input which is a signal (Moore, K., 1993).

The basic properties and features of RC, AC and NN are as following:

AC and NN controllers modify the systems (controller parameters) not the control inputs. RC is intended for continuous operations and it starts from stopping point (final condition). It is usually used in applications that don't have specified start and finish times. Common applications of repetitive controllers can be existed in control of computer's hard disk drives (Bristow, D. A., 2006). Finally, *"For large data the fast convergence may be difficult to guarantee by them whereas ILC converges in just a few iterations"* (Hunter, K. J., 2003).

3.9 ITERATIVE LEARNING CONTROLLER (ILC)

The main aim of controller is to find the feed forward signal which has task to track reference signal, in order to improve the performance by eliminate and attenuate the repeated disturbance (Bristow, D. A., 2006). Owing to the normal controllers that need feedback in order to deal with input signals and disturbance, this deal will always have a lag in tracking due to the nature of its elements and the systems. This lag can be eliminated by using feed forward technique. This technique is suitable for the signals which are measurable not for the disturbance and repeated disturbance. Because of ILC is able to anticipate and compensate disturbance signals in next iterations from previous iterations, it is the best choice for fast performance and perfect tracking. Moreover, ILC does not need high knowledge about nature and parameters of the plants (motors, actuators, etc.) which are controlled by it and ILC can be used for the open loop systems and closed loop systems. There are various definitions of iterative learning controller in the books and literatures; one of them is "*ILC is an approach to improve the transient response performance of an unknown / uncertain hardware system that operates repetitively over a fixed time interval by using the previous actual operation data to compensate for uncertainty*" (Ahn, H-S., 2007). This approach has key for good results which is the repetition or iteration. In addition, ILC is mainly used to get the inverse of predetermined effect, such as fixed time point, repetitive desire trajectory, uniform sampling, etc. (Ahn, H-S., 2007). Disturbance attenuation, robust stability and noise rejection are the most important specification of track following controller design. Because these specifications are conflict with each other, the procedure of designing these controllers demands high number of trial and errors, also, the system considered

impractical due to high order controller design (Doh, T.-Y., 2006). That is another reason why the ILC is best choice.

The learning controller is an error correction algorithm and a memory that stores the previous error information. ILC computes the error between the actual output and the reference, then, computes a new input which is stored in a memory for future operation. It is worth to say, *"ILC is intended to vanish periodic disturbances in the inputs and it does not have any effect on non-periodic disturbances such as torque ripples caused by load side because the time period is define as the basic period in ILC, and the non-periodic does not share that basic time period with others. Therefore, it is impossible to find its time period because from its nature, it is non-periodic and have non-integer multiples"* (Qian, W., 2005). In addition, ILC can be planted to any control system without remodeling the whole control system. The block diagram of iterative learning control is given in Figure 3.15.

Figure 3. 15: Block Diagram of Iterative Learning Controller

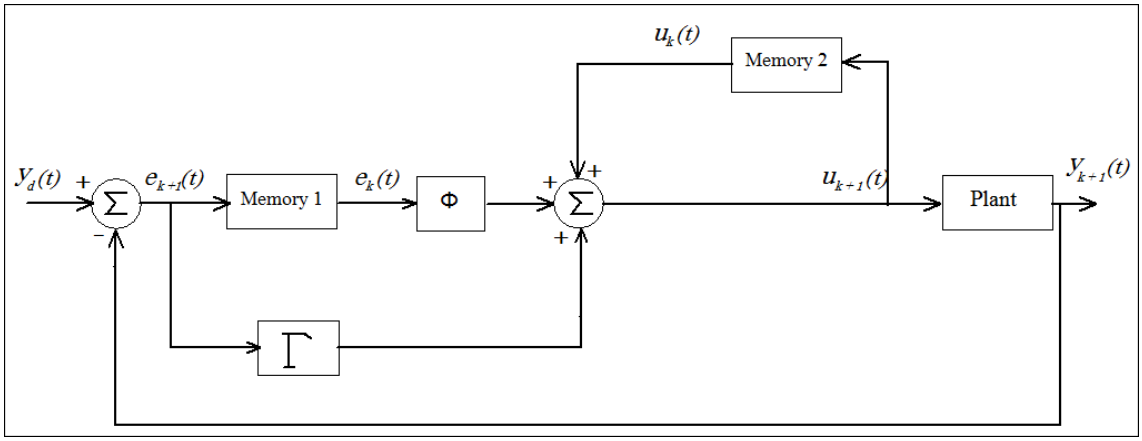

Source: Lam B., 2000

Finally, based on the algorithms used in design of Iterative learning controller, ILC can be classified into types such as P-type ILC, PD-type ILC and PID-type ILC. The types and its algorithms are shown in Tables 3.4.

Tables 3.4: Types of ILC and algorithms

Types	Algorithms
P-type	$u_{(k+1)}(t) = u_{(k)}(t) + \Phi * er_{(k)}(t+1) + \Gamma * er_{(k+1)}(t)$
PD-type	$u_{(k+1)}(t) = u_{(k)}(t) + k_p * er_{(k)}(t+1) + k_d * [er_{(k+1)}(t+1) - er_{(k)}(t)]$
PID-type	$u_{(k+1)}(t) = u_{(k)}(t) + k_p * er_{(k)}(t+1) + k_d * [er_{(k+1)}(t+1) - er_{(k)}(t)] + k_i \int er_{(k)}(\tau) d\tau$

where Φ is the previous cycle feedback gain (PCF), Γ is the current cycle feedback gain (CCF), $u(t)$ is the input control and $er_{(k)}$ is the error at iteration k, k_p is proportional gain**, ,** k_d is derivative gain and k_i is integral gain. According to (Ahn, H., 2005) and **(**Swevers, J., 2014**),** the asymptotic stability condition of P-type and PD-type is given in Equations 3.65 and 3.66 respectively:

$$|1 - \Phi \gamma_1| < 1 \quad \textbf{(3.65)}$$

$$|1 - (k_p + k_d)\gamma_1| < 1 \quad \textbf{(3.66)}$$

where γ_1 is the first non-zero Markov parameter.

4. REDUCTION OF COMMUTATION TORQUE RIPPLES

4.1 CURRENT CONTROL

Torque analysis during commutation period shows that torque in this period depends on the phase currents and back EMFs as in Equation 3.62. Therefore, the controller should deal with elements which are affected in this period and not directly involved with commutation. That means the un-commutated current phase and its back EMF are appropriate to achieve that. Therefore, the current control loop is suitable for reducing un-commutated current ripples in order to reduce torque ripple. Thus, there are two controllers employed to reduce torque ripple, conventional dead-beat current controller is applied during normal period and commutation period whereas iterative learning controller is just applied for commutation period

4.2 DEAD-BEAT CONTROLLER

Dead-beat controller is a control strategy in discrete time system and the aim of this strategy is to make each initial state of the system as zero in shortest possible period (Quan, 2013). In this work, during normal period, the dead-beat current controller is used to determine the error between the reference current and the measured current at the beginning of each sampling period of PWM and then to compute new reference voltage for PWM drive. For commutation period, two different controllers are used to compute the reference voltage.

For finding the formula of dead-beat controller, it is necessary to find new sector which includes whole un-commutated current with its ripple. From Figure 3.14, which shows the sequence of BLDC motor's commutation during one electrical cycle, the un-commutated current, and back EMF for each sector and new sectors can be concluded. The result of that is represented in Figure 4.1and Table 4.1.

Figure 4.1: New sectors (Currents and back EMFs)

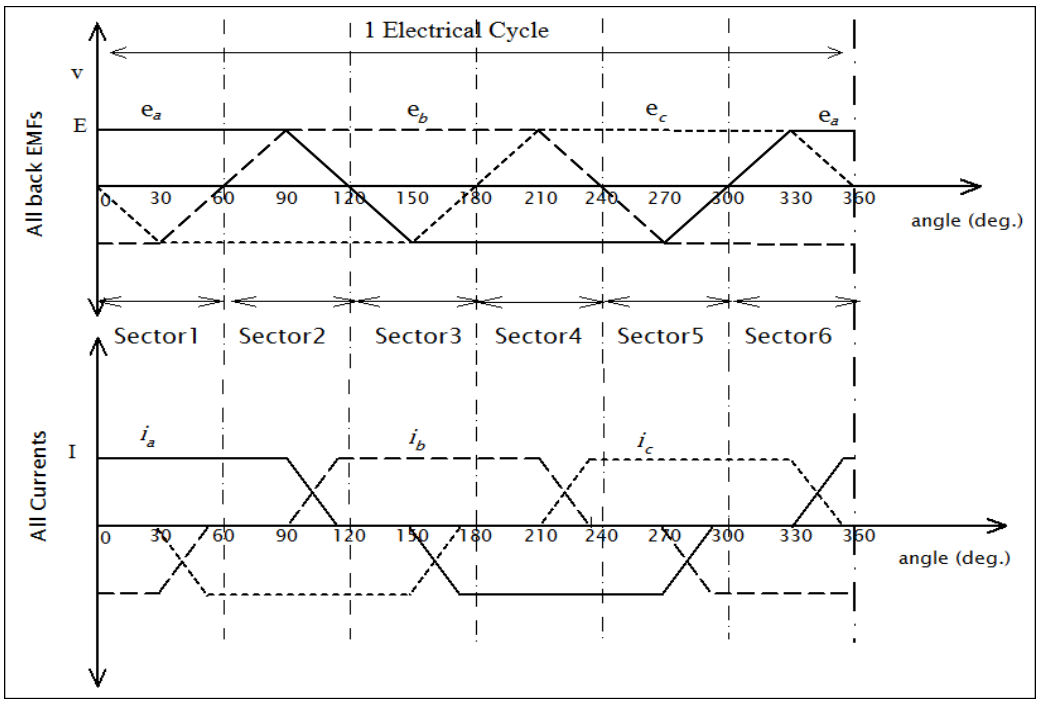

Table 4.1: Un-commutated currents, back EMFs in sectors and new sectors

Sector	θ_e	Un-com. Current	EMF	New sector	θ_e	Un-com. current i	EMF E
1	$30^0 < \theta_e <= 90^0$	$-i_b$	$-e_b$	1	$0^0 < \theta_e <= 60^0$	i_a	e_a
2	$90^0 < \theta_e <= 150^0$	i_a	e_a	2	$60^0 < \theta_e <= 120^0$	$-i_c$	$-e_c$
3	$150^0 < \theta_e <= 210^0$	$-i_c$	$-e_c$	3	$120^0 < \theta_e <= 180^0$	i_b	e_b
4	$210^0 < \theta_e <= 270^0$	i_b	e_b	4	$180^0 < \theta_e <= 240^0$	$-i_a$	$-e_a$
5	$270^0 < \theta_e <= 330^0$	$-i_a$	$-e_a$	5	$240^0 < \theta_e <= 300^0$	i_c	e_c
6	$330^0 < \theta_e <= 30^0$	i_c	e_c	6	$300^0 < \theta_e <= 360^0$	$-i_b$	e_b

Firstly, the formula, which is used to control the reference voltage for dead-beat controller, should be found. The inductor current is given by

$$L * \frac{di}{dt} = (-R * i - \mathrm{E} + V^*) \qquad \textbf{(4.1)}$$

where i is the measured current and this current is used in controller to determine the current error, V^* is the reference voltage that is applied to PWM drive, E is the flat magnitude of back EMF and R is the phase resistance. A discrete time approximation of Equation 4.1 yields,

$$i_{(k+1)} = i_{(k)} + \frac{1}{L} * (-R * i - \mathrm{E} + V^*) * T_p \quad \textbf{(4.2)}$$

$$er_{(k)} = i^*_{(k)} - i_{(k)} \quad \textbf{(4.3)}$$

where T_p is the PWM period (controller's sampling), er is the current error, k indicates the time instance and i^* is the reference current.

$$er_{(k+1)} = i^*_{(k+1)} - i_{(k+1)} \quad \textbf{(4.4)}$$

Using 4.2 in 4.4 and arranging the results, the error equation is given by:

$$er_{(k+1)} = i^*_{(k+1)} - i_{(k)} - \frac{T_p}{L} * (-R * i - \mathrm{E} + V^*) \quad \textbf{(4.5)}$$

Assuming the reference current is constant, then:

$$er_{(k+1)} = i^*_{(k)} - i_{(k)} - \frac{T_p}{L} * (-R * i - \mathrm{E} + V^*) \quad \textbf{(4.6)}$$

$$er_{(k+1)} = er_{(k)} - \frac{T_p}{L} * (-R * i - \mathrm{E} + V^*) \quad \textbf{(4.7)}$$

If the control signal is assigned as

$$V^*_{(k)} = R * i_{(k)} + E_{(k)} + (er_{(k)}) * L/T_p\,, \quad \textbf{(4.8)}$$

then, the next error will be zero, that means $er_{(k+1)} = 0$.

Equation 4.8 shows the output signal of dead-beat controller without controlling the reference voltage during commutation period. The block diagram for this controller is presented in Figure 4.2.

Figure 4.2: Dead-beat Controller

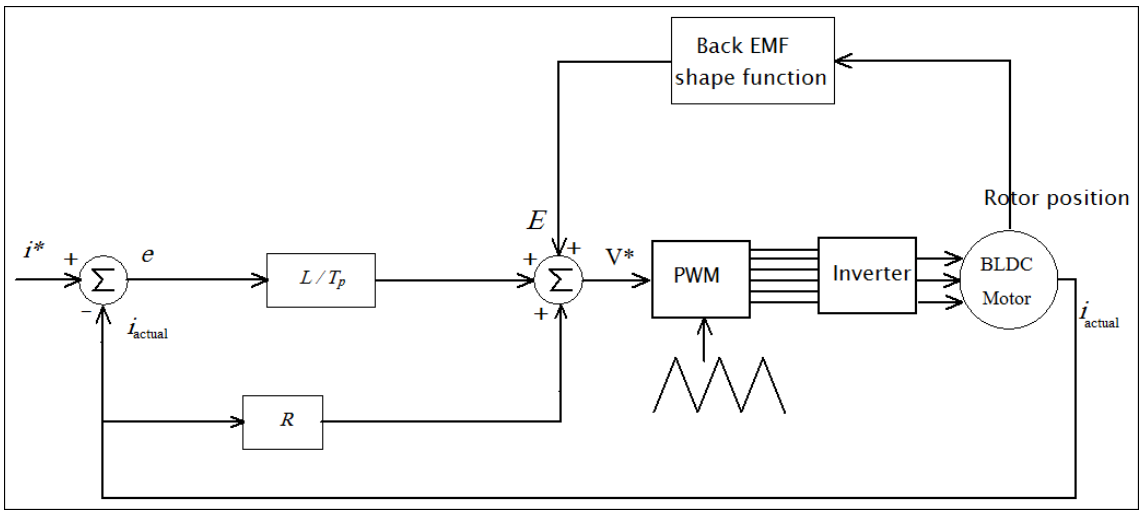

Secondly, the formula for control reference voltage during commutation period can be found by a similar way to previous one. Un-commutated current during commutation is given by Equation 3.24 and the discrete time approximation of this equation yields,

$$i_{(k+1)} = i_{(k)} + \frac{1}{3*L} * [-3* R * i_1 + 2 * V_1 - V_2 - V_3 - 2 * e_1 + e_2 + e_3] * T_p \qquad \textbf{(4.9)}$$

Then, the error can be obtained

$$er_{(k+1)} = i^*_{(k)} - i_{(k)} + \frac{T_p}{3*L} * [3* R * i_1 - 2 * V_1 + V_2 + V_3 + 2 * e_1 - e_2 - e_3] \qquad \textbf{(4.10)}$$

The supply voltages for each sector can be concluded in a similar fashion and they are indicated in Figure 4.3.

Figure 4.3: Applied voltages in new sectors

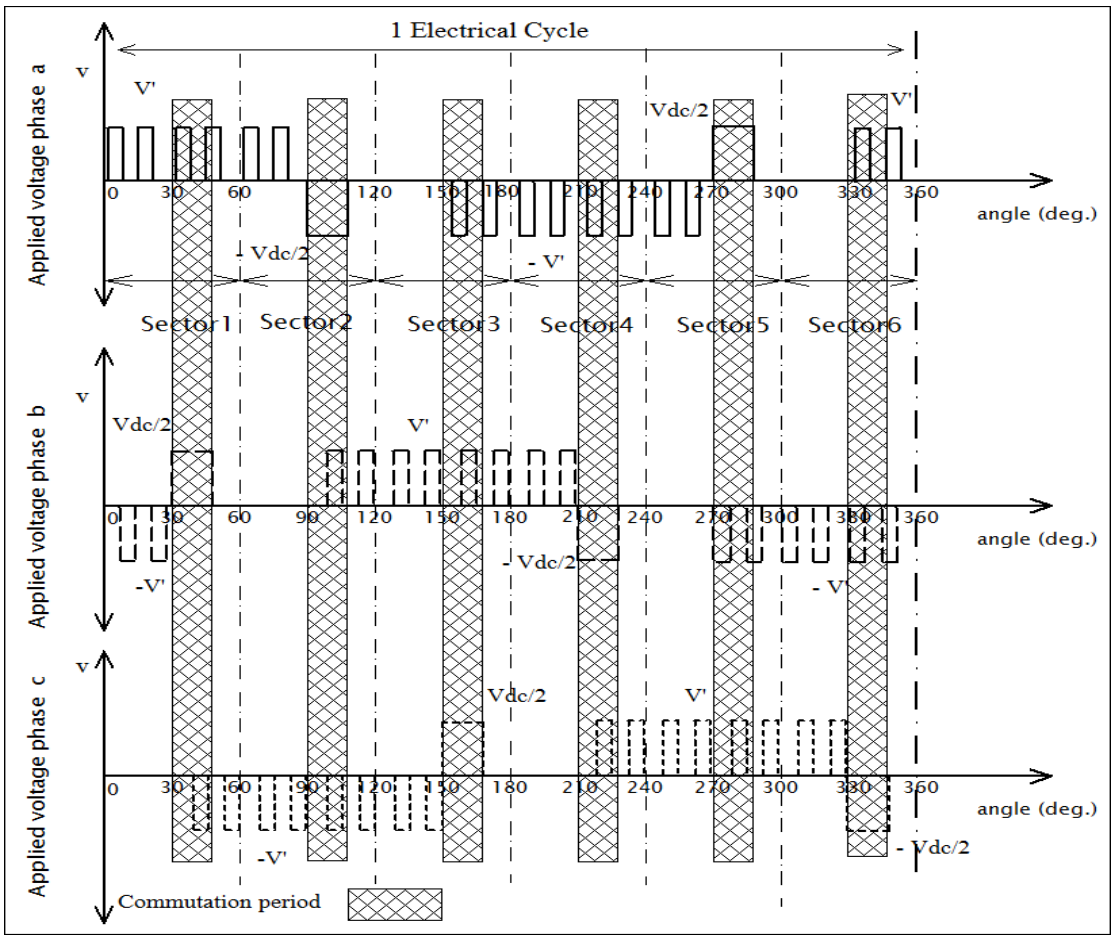

For sector 1, $V_a = V^*, V_c = -V^*$ and $V_b = \frac{V_{dc}}{2}$ also $i_1 = i_a$, $i_2 = i_b, i_c = -(i_a + i_b)$, $\mathrm{e}_1 = \mathrm{e}_a, \mathrm{e}_2 = \mathrm{e}_b$ and $\mathrm{e}_3 = \mathrm{e}_c$. Then, the current error for new sector 1 during commutation period is given by:

$$er_{(k+1)} = i^*_{(k)} - i_{a(k)} + \frac{T_p}{3*L} * [3* R * i_a - 3 * V^* + \frac{V_{dc}}{2} + 2 * \mathrm{e}_a - \mathrm{e}_c - \mathrm{e}_b] \quad \textbf{(4.11)}$$

If the reference voltage is assigned as

$$V^* = \frac{1}{3} * [\frac{V_{dc}}{2} + 2 * \mathrm{e}_a - \mathrm{e}_c - \mathrm{e}_b + 3 * (R * i_a + \frac{L}{T_p} er_{(k)})], \quad \textbf{(4.12)}$$

then, the error for the next time instance will be zero, i.e. $er_{(k+1)} = 0$.

The equation 4.12 is the input voltage that should be controlled during commutation period in new sector 1. In summary, Table 4.2 gives all details for new sectors and the reference voltage that should be controlled during commutation period**.**

Table 4.2: New sectors' details during commutation

New sector	V_a	V_b	V_c	i_1	i_2	i	Output of dead-beat controllr
1	V^*	$\frac{V_{dc}}{2}$	$-V^*$	i_a	i_b	i_a	$V^*=\frac{1}{3}*[\frac{V_{dc}}{2}+2*e_a-e_c-e_b+3*(R*i+\frac{L}{T_p}er_{(k)})]$
2	$-\frac{V_{dc}}{2}$	V^*	$-V^*$	i_b	i_a	$-i_c$	$V^*=\frac{1}{3}*[\frac{V_{dc}}{2}-2*e_c+e_a+e_b+3*(R*i+\frac{L}{T_p}er_{(k)})]$
3	$-V^*$	V^*	$\frac{V_{dc}}{2}$	i_b	i_c	i_b	$V^*=\frac{1}{3}*[\frac{V_{dc}}{2}+2*e_b-e_c-e_a+3*(R*i+\frac{L}{T_p}er_{(k)})]$
4	$-V^*$	$-\frac{V_{dc}}{2}$	V^*	i_c	i_b	$-i_a$	$V^*=\frac{1}{3}*[\frac{V_{dc}}{2}-2*e_a+e_c+e_b+3*(R*i+\frac{L}{T_p}er_{(k)})]$
5	$\frac{V_{dc}}{2}$	$-V^*$	V^*	i_c	i_a	i_c	$V^*=\frac{1}{3}*[\frac{V_{dc}}{2}+2*e_c-e_a-e_b+3*(R*i+\frac{L}{T_p}er_{(k)})]$
6	V^*	V^*	$-\frac{V_{dc}}{2}$	i_a	i_c	$-i_b$	$V^*=\frac{1}{3}*[\frac{V_{dc}}{2}-2*e_b+e_c+e_a+3*(R*i+\frac{L}{T_p}er_{(k)})]$

4.2.1 SIMULATION RESULTS FOR DEADBEAT CONTROLLER

Figures 4.4, 4.5 and 4.6 show the simulation results for the dead-beat controller without controlling voltage during commutation period for 500 RPM, 1500 RPM and 3000 RPM respectively. The motor parameters are given in Table 4.3, DC supply voltage is 24V and the reference current is 3A. These figures show the waveforms of phase currents, reference voltage (input control) and the torque. The results indicate how the un-commutated current is affected by appearing spikes and dips in its waveforms, this deviation is reflected on torque by existing the ripples. Furthermore, the spikes and dips are increased at high speed.

Table 4.3: Relevant parameters of BLDC motor

Parameters	Symbol	Value	Unit
Motor back (EMF) constant	k_e	0.0339	Voltage . sec/rad
Motor torque constant	k_t	6.2e-3	N . m/amp
Stator resistance	R	0.18	Ohm
Stator inductance	L	1.43e-3	Henry
Motor inertia	J	1.024e-4	Kg .m^2
Motor viscous friction	B	1e-6	N . m/rad/sec
Number of poles	P	10	Unit

Figure 4.4: Simulation results of dead-beat controller without controlling during commutation for W_R=500 RPM

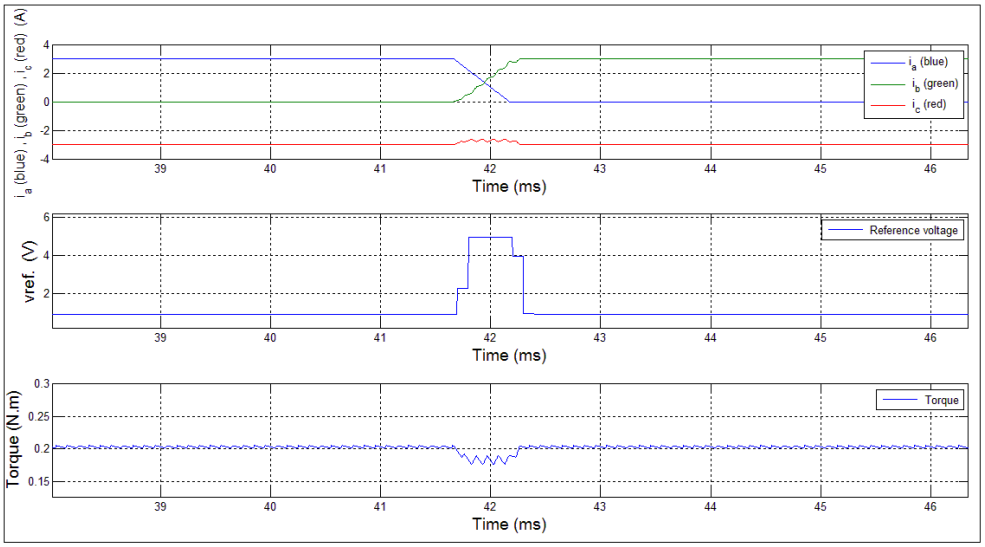

Figure 4.5: Simulation results of dead-beat controller without controlling during commutation for W_R=1500 RPM

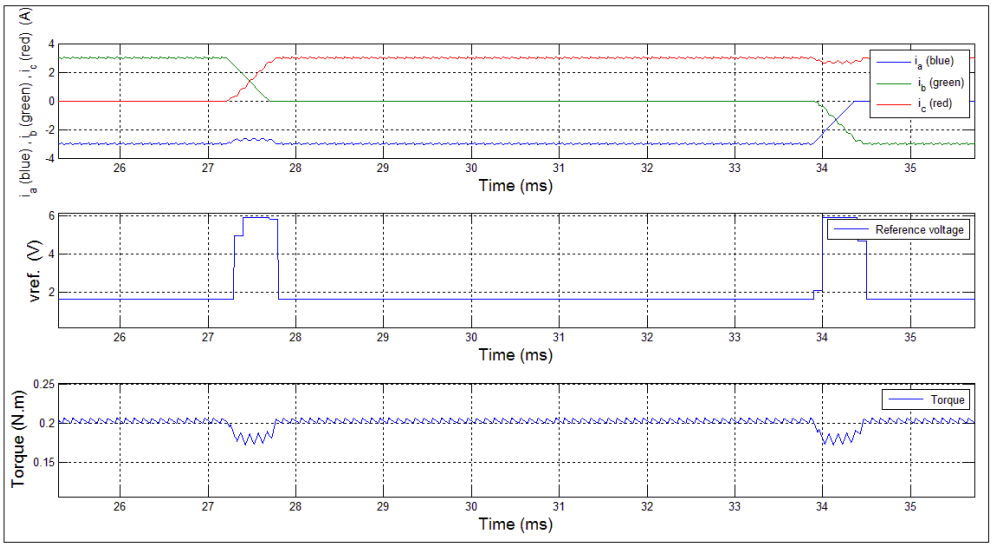

Figure 4.6: Simulation results of dead-beat controller without controlling during commutation for W_R=3000 RPM

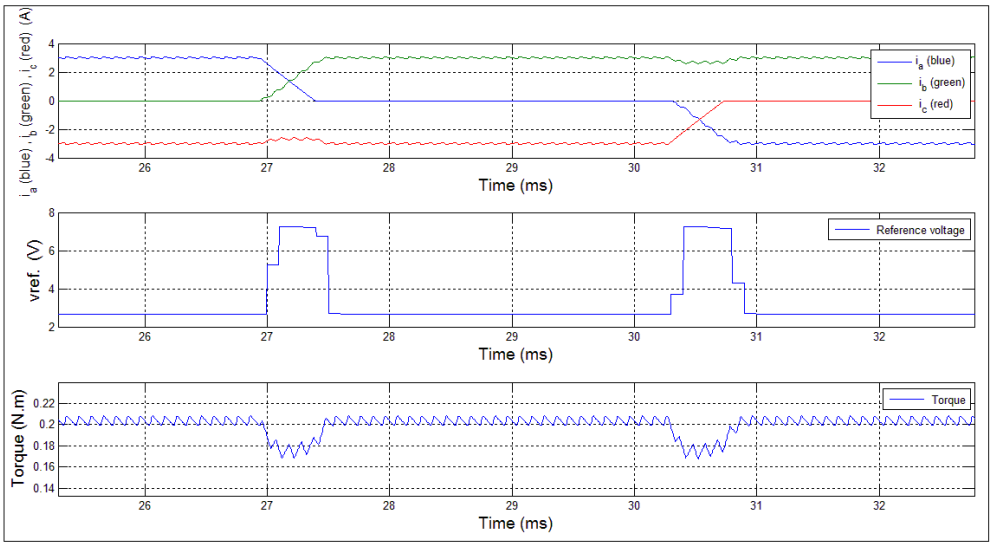

Figures 4.7, 4.8 and 4.9 show the simulation results for dead-beat controller with controlling reference voltage during commutation period for 500 RPM, 1500 RPM and 3000 RPM respectively. These figures show the waveforms of phase currents, reference voltage (input control) and the torque. The results indicate how the un-commutated

current waveform is better than the previous results because the reference signal is controlled during normal and commutation period separately. Because of that, the torque ripples typically appear less.

Figure 4.7: Simulation results of dead-beat controller with controlling during commutation for W_R=500 RPM

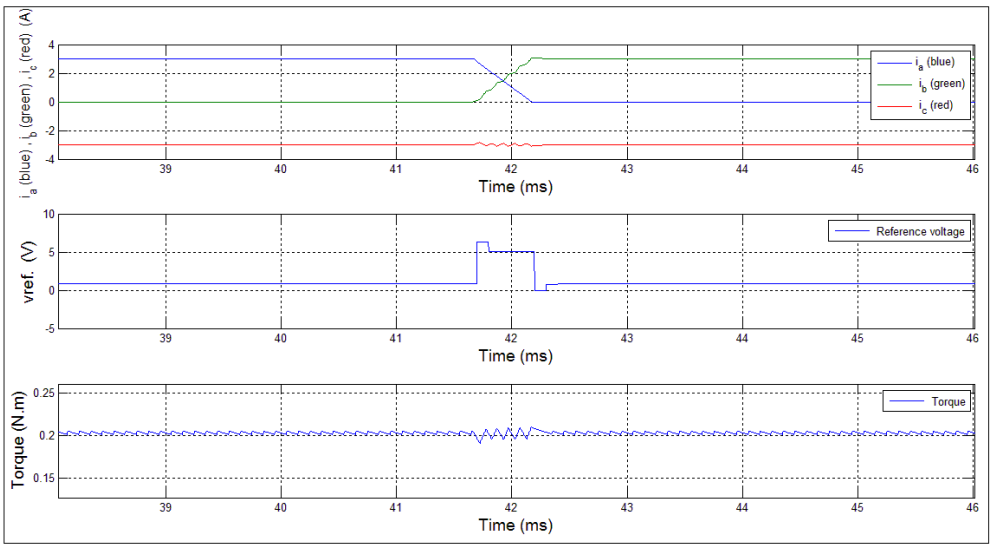

Figure 4.8: Simulation results of dead-beat controller with controlling during commutation for W_R= 1500 RPM

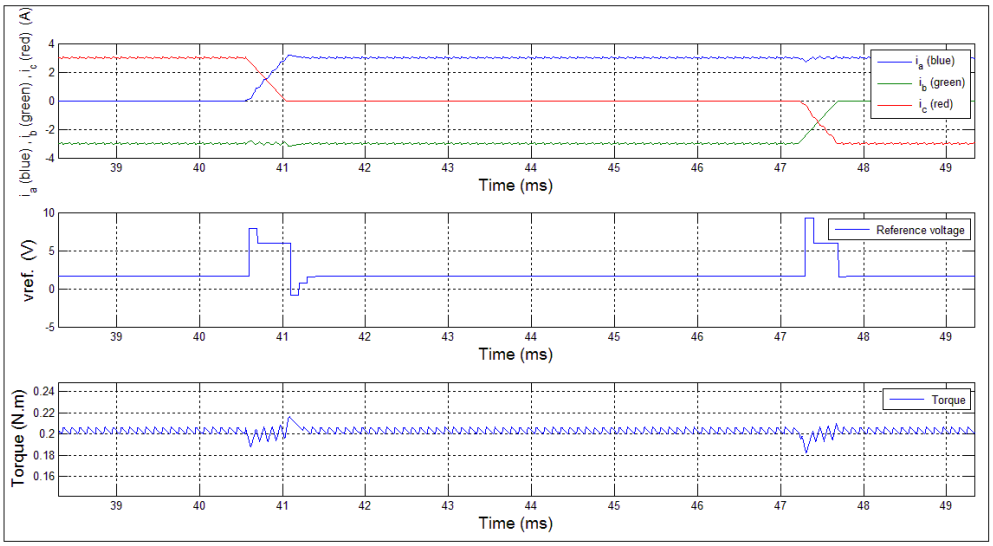

Figure 4.9: Simulation results of dead-beat controller with controlling during commutation for W_R= 3000 RPM

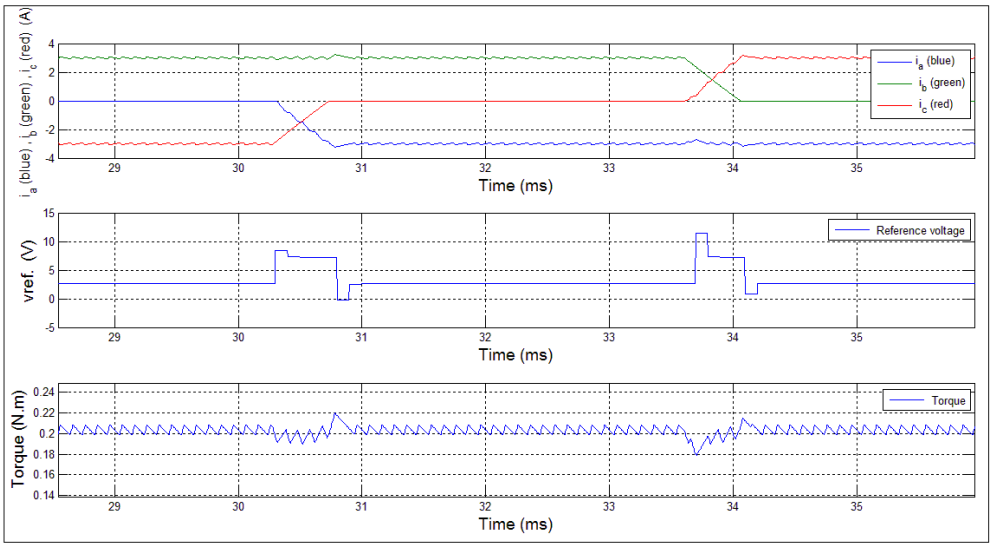

Figure 4.10 shows the comparison between the two simulation results with/without controlling during commutation of 1500 RPM. It is obvious that the controller gives better results when the reference voltage is controlled during both periods. Moreover, it can be observed that the torque is smoother and its ripple less than the case of without controlling during commutation period. The red one is for controlling during both periods.

Figure 4.10: Comparison between with/without controlling during commutation for W_R= 1500 RPM

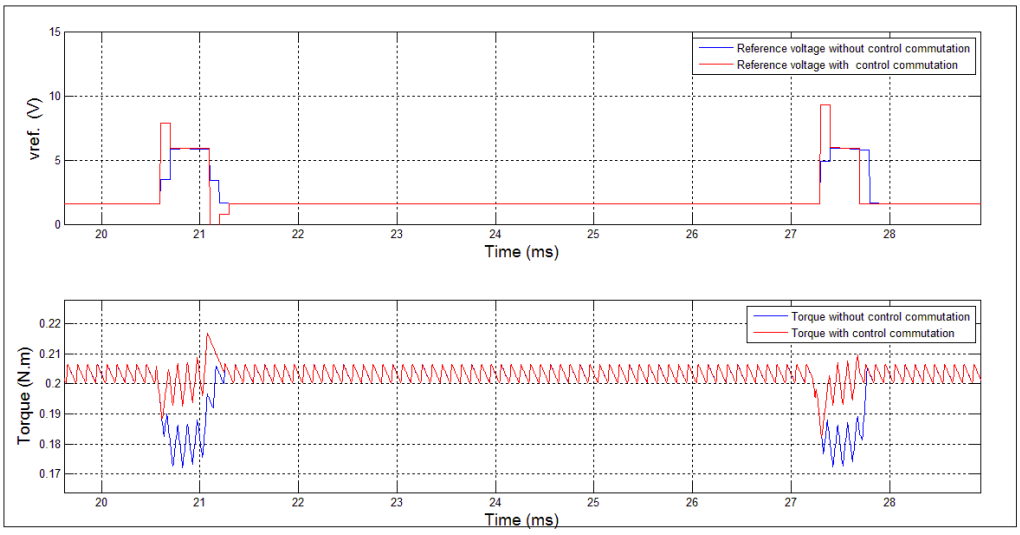

4.2.2 PROBLEM OF DUTY CYCLE COMPUTATION

When the dead-beat controller is applied during normal and commutation period, there is a problem appeared in torque waveforms. Irregular dips and spikes are existed at beginning and ending of commutation. This drawback is appeared due to the overlap of computation duty cycle for PWM period. For example, before commutation period ends, the controller computes the reference voltage and that voltage is started to be applied. It is applied during commutation period but it is also finished during normal period with same duty cycle because it cannot be changed until the next PWM period starts which therefore produces ripple. Similarly, in some of normal periods, the computed voltage reference is applied during the two periods which produces ripple. That means, there are 4 types of duty cycles should be computed in controller during normal period, commutation period and for the two mixed periods. The two mixed period are just laid before commutation starts and ends for one PWM period as in Figure 4.11.

Figure 4.11: Problem of Mixed Periods

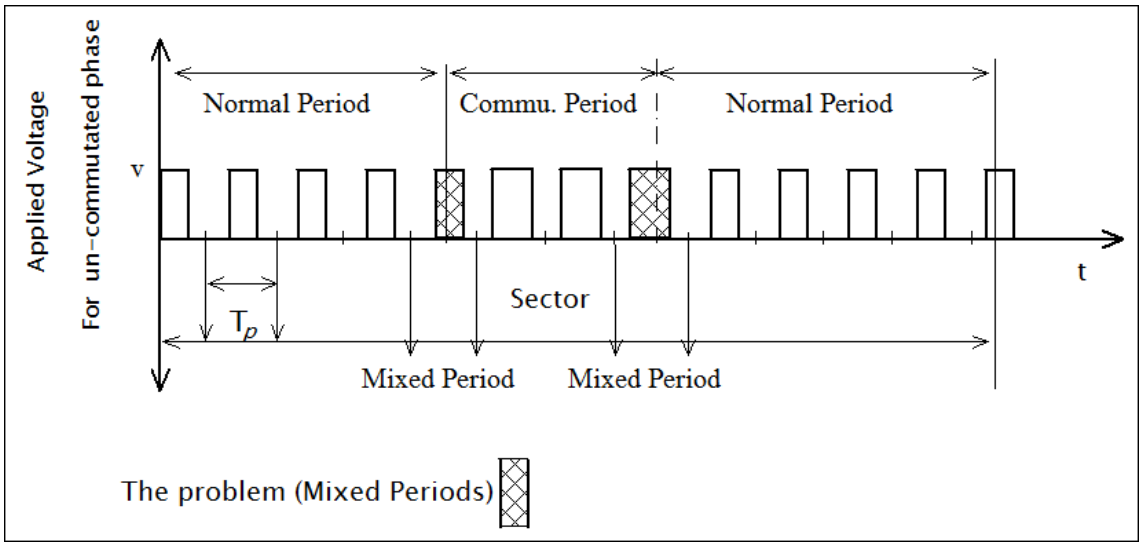

To overcome that, the duty cycle should be modified during mixed period. This modification can be achieved by predicting the beginning and ending of commutation period. Then, new reference voltage is applied for the mixed period. To predict the beginning of commutation, let assume $\hat{\theta}_{e\,(k)}$ is an angle for PWM's signal can be laid in

any sector and $\hat{\theta}_{e\,(k+1)}$ is the angle of starting commutation and these angles are for the two sequential $PWM_{(k)}$ and $PWM_{(k+1)}$ respectively, they are stated in Figure 4.12. The prediction can be performed for the next time instance.

$$\hat{\theta}_{e\,(k+1)} = \hat{\theta}_{e\,(k)} + \omega_{e\,(k)} * T_p \qquad \textbf{(4.13)}$$

Figure 4.12: Prediction the beginning of commutation

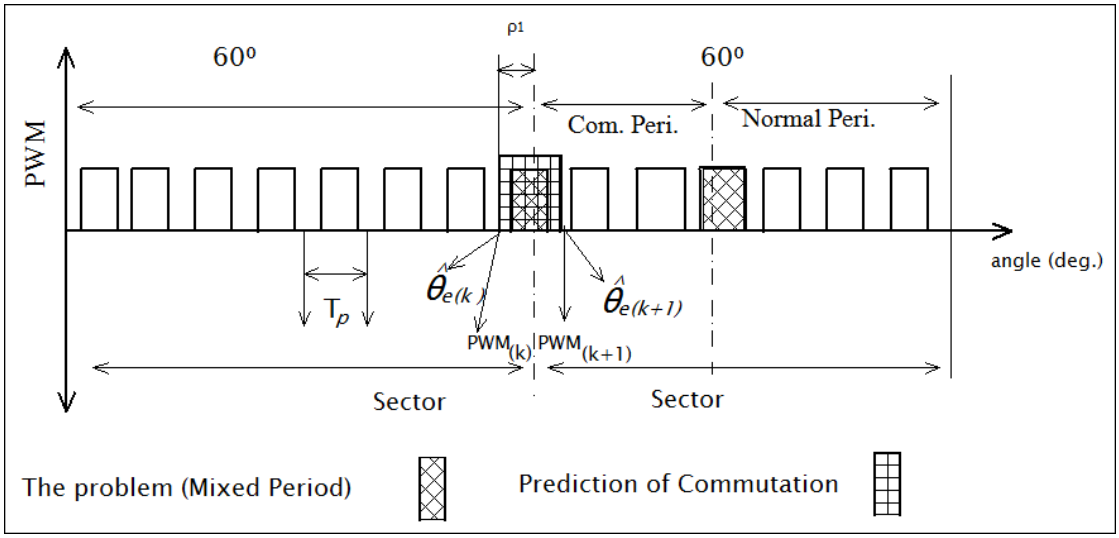

When sector changes in between $PWM_{(k)}$ and $PWM_{(k+1)}$, the commutation starts in the next PWM period. Moreover, when the commutation period is going to begin, it can be predicted. As in Figure 4.1, the angles of commutation for each sector are 30^0, 90^0, 150^0, 210^0, 270^0, 330^0 and the difference between them is 60^0. Therefore, the value of $\hat{\theta}_{e\,(k)}$ is changed between 0^0 and 60^0. In other words, if $\hat{\theta}_{e\,(k+1)}$ >60^0, then, the commutation is started. ρ_1 gives the percentage of the un-commutating time in a mixed PWM period at beginning of commutation as in Equation 4 .14.

$$\rho_1 = \frac{60^0 - \hat{\theta}_{e\,(k)}}{\hat{\theta}_{e\,(k+1)} - \hat{\theta}_{e\,(k)}} . \qquad \textbf{(4.14)}$$

Thus, the formula which is used to compute the duty cycle of PWM during mixed period at beginning of commutation is depended on ρ_1 as in Equation 4.15.

$$V^* = \left(V^*_{\ normal\ period} \right) * \rho_1 + (V^*_{(commutation)}) * (1 - \rho_1) \quad \textbf{(4.15)}$$

For predicting the ending of the commutation period, the outgoing current should be measured and predicted. The dynamics of the outgoing current is given by:

$$L * \frac{di_{out}}{dt} = (-R * i_{out} - e_{out} + V_{out}) \quad \textbf{(4.16)}$$

where i_{out}, e_{out} and V_{out} are current, back EMF and voltage for the coil which is separated from supply voltage during commutation period. A discrete time approximation of Equation 4.16 yields,

$$i_{out(k+1)} = i_{out(k)} + \frac{1}{L} * (-R * i_{out(k)} - e_{out(k)} + V_{out(k)}) * T_p \ . \quad \textbf{(4.17)}$$

Considering T_c is the remaining commutation time for ending of the commutation period and replacing the equation of outgoing current during commutation in Equation 4.17, the outgoing current equation becomes:

$$i_{out(k+1)} = i_{out(k)} + \frac{1}{3*L} * (-3 * R * i_{out(k)} - 2 * e_{out(k)} + 2 * V_{out(k)}) * T_c \quad \textbf{(4.18)}$$

then,

$$T_c = \frac{i_{out\,(k+1)} - i_{out(k)}}{(-3*R*i_{out(k)} - 2*e_{out(k)} + 2*V_{out(k)})} \quad \textbf{(4.19)}$$

T_c tells how much time is needed for ending the commutation period and ρ_2 gives the percentage of the commutating time in mixed period as in Equation 4.20.

$$\rho_2 = T_c \ / \ T_p \quad \textbf{(4.20)}$$

The commutation period will end in next period if the sign of the predicted outgoing current in next PWM period is different with sign of outgoing current in previous PWM period as in Figure 4.13.

Figure 4.13: Prediction the ending of commutation

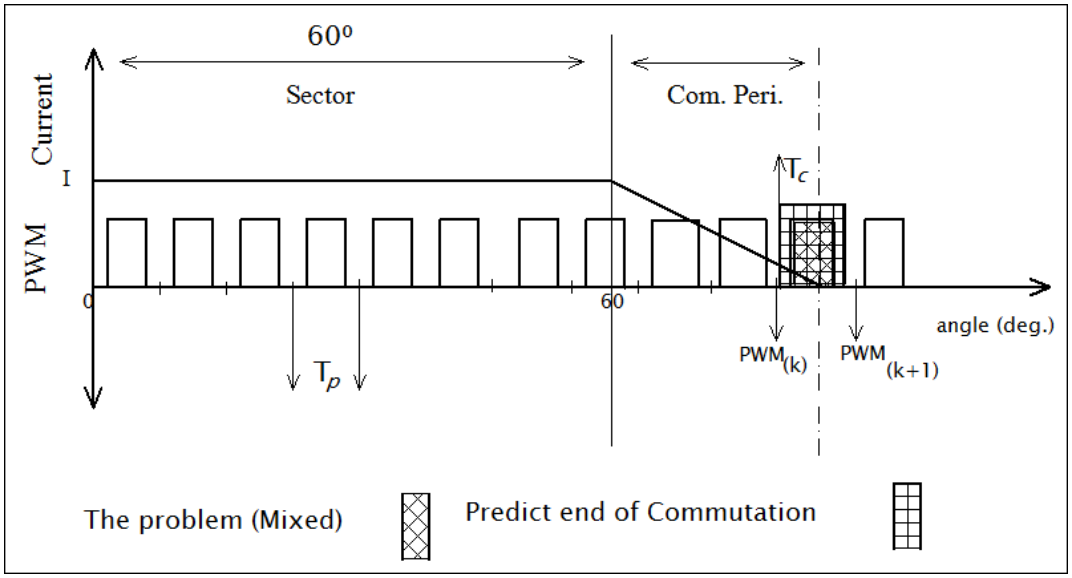

Finally, the formula, which is computed the modification of duty cycle during mixed period at ending of commutation is depended on ρ_2 as in Equation 4.21**.**

$$V^* = \left(V^*_{normal\ period}\right) * (1 - \rho_2) + (V^*_{(commutation)}) * \rho_2 \qquad \textbf{(4.21)}$$

4.2.3 SIMULATION RESULTS WITH MIXED PERIODS

Figures 4.14, 4.15 and 4.16 show the waveforms of phase currents, reference voltage (input control) and the torque with new modification of PWM during mixed periods for 500 RPM, 1500 RPM and 3000 RPM respectively. These figures indicate how the un-commutated current dips and spikes hardly appear due to the modification of PWM during mixed periods. It can be also found that the commutation torque ripple is attenuated.

Figure 4.14: Simulation results of dead-beat controller with PWM modification for W_R = 500 RPM

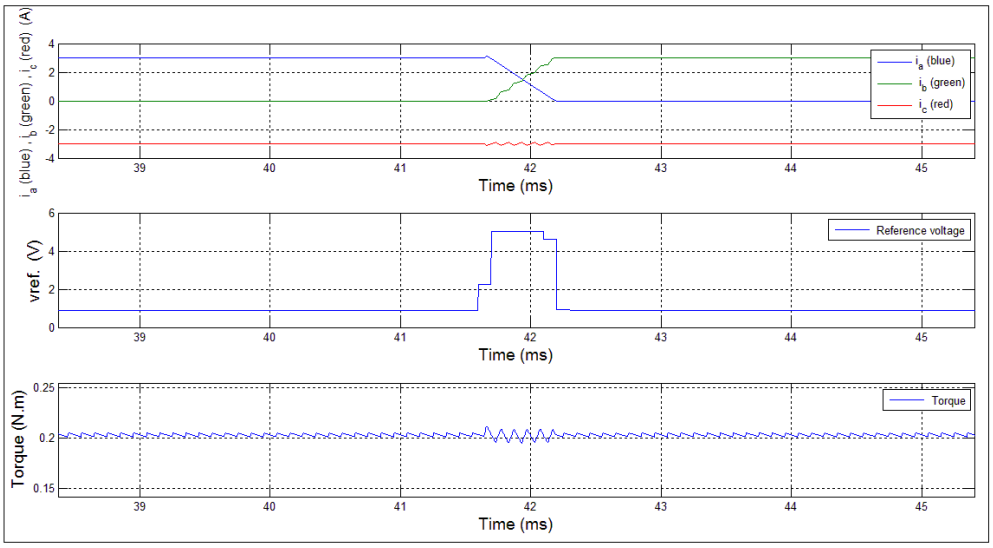

Figure 4.15: Simulation results of dead-beat controller with PWM modification for W_R = 1500 RPM

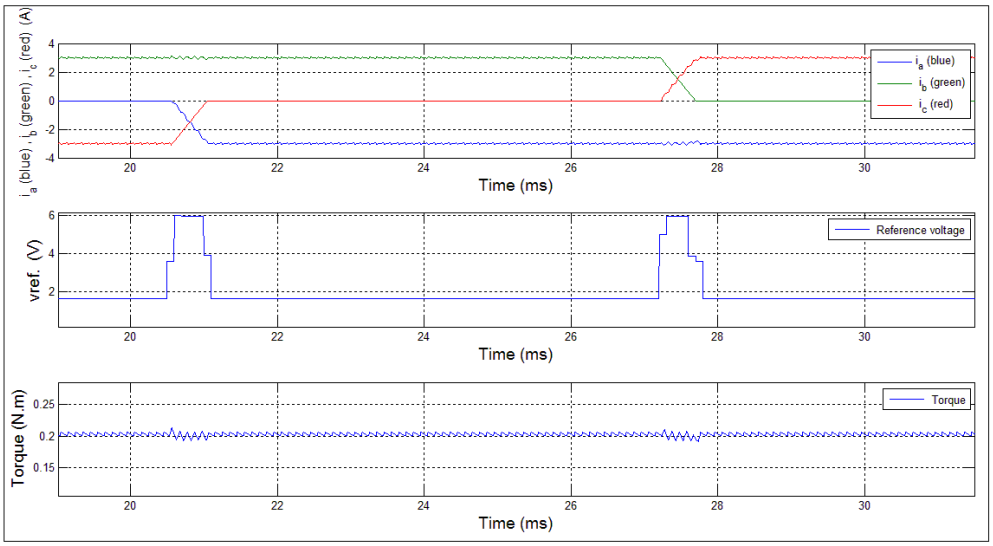

Figure 4.16: Simulation results of dead-beat controller with PWM modification for W_R = 3000 RPM

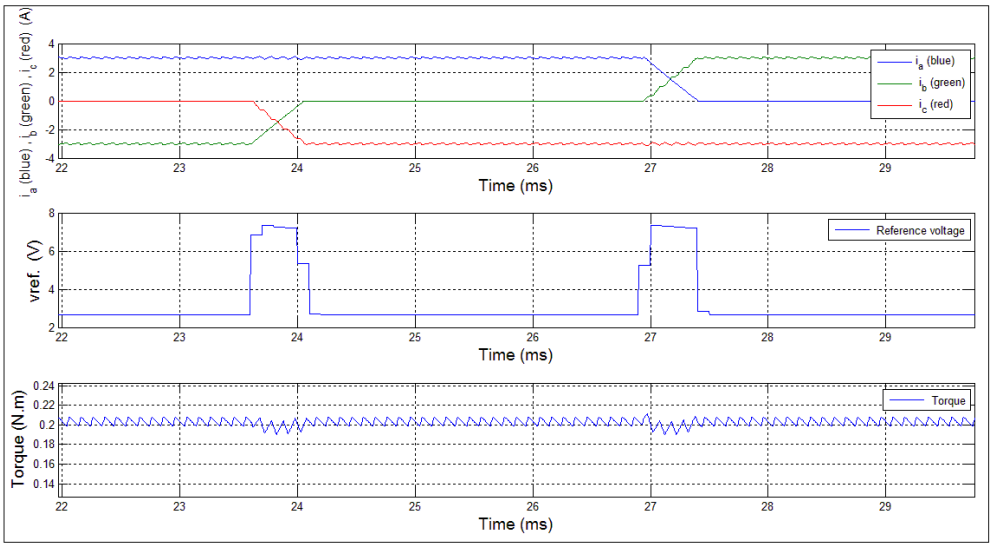

The comparison between the two simulation results with/without PWM modification for 1500 RPM is given in Figure 4.17. It is clear that the controller gives better results when it is applied with new modification (red) because the irregular dips and spikes in torque waveform are suppressed.

Figure 4.17: Comparison between with/without PWM modification for W_R = 1500 RPM

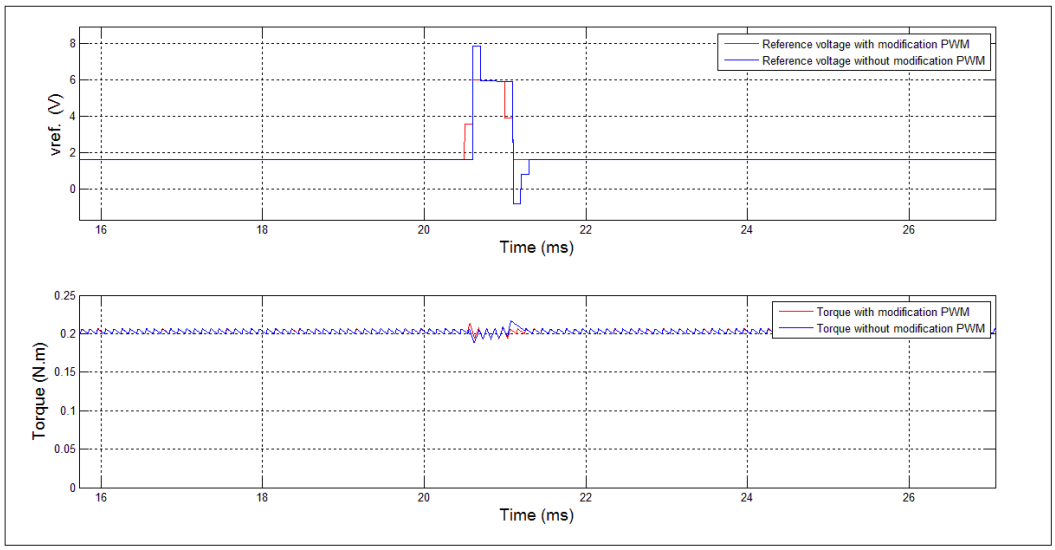

4.3 PROPOSED CONTROLLER

Figure 2.1 shows block diagram of the current control loop which is used as proposed controller in this thesis. There are two controllers. One of them, which is used during normal period and the mixed periods, is the dead-beat current controller. The other one, which is used for the same mixed periods and commutation period, is the iterative learning controller. The controller signal for proposed controller during commutation period is given by:

$$V^*_{(commutation)} = V_{ref.\ (dead-beat)} + V_{ref.\ (ILC)} \quad \textbf{(4.22)}$$

where $V^*_{(commutation)}$ is the reference voltage which is controlled during commutation period, $V_{ref.\ (dead-beat)}$ is the control voltage which is applied from dead-beat controller with respect to each sector and $V_{ref.\ (ILC)}$ is the additional compensating voltage which is applied from ILC. Consequently, for the mixed periods, which are explained in Section 4.2.2**,** the input control equation for the proposed controller during commutation period is given in Table 4.4.

Table 4.4: Input control equations for proposed controller

Periods	Input control equation
First mixed period	$V^* = \left(V^*_{(normal\ period)}\right) * \rho_1 + \left(V^*_{(commutation)}\right) * (1 - \rho_1)$
Commutation period	$V^* = V^*_{(commutation)}$
Second mixed period	$V^* = \left(V^*_{(normal\ period)}\right) * (1 - \rho_2) + \left(V^*_{(commutation)}\right) * \rho_2$

When ILC is applied, it provides the compensating voltage for the next iteration according to Equation 4.22.

$$V_{(k+1)}(t) = V_{(k)}(t) + \Phi * er_{(k)}(t) + \Gamma * er_{(k+1)}(t) \quad \textbf{(4.22)}$$

$er_{(k)}$ is the torque error at iteration k, this error is calculated by finding the maximum torque ripple at any iteration and it is used in algorithm of the ILC in the simulation.

4.3.1 SIMULATION RESULTS OF PROPOSED CONTROLLER

Figures 4.18, 4.19 and 4.20 show the simulation results when the proposed controller is applied with $\Phi = 5$ and $r = 0$ for 500 RPM, 1500 RPM and 3000 RPM respectively. In these figures, it is clear that the ripple in un-commutated current is minimized. Thus, torque waveform is appeared smoother than when dead-beat controller is applied alone.

Figure 4.18: Simulation results of proposed controller for W_R = 500 RPM

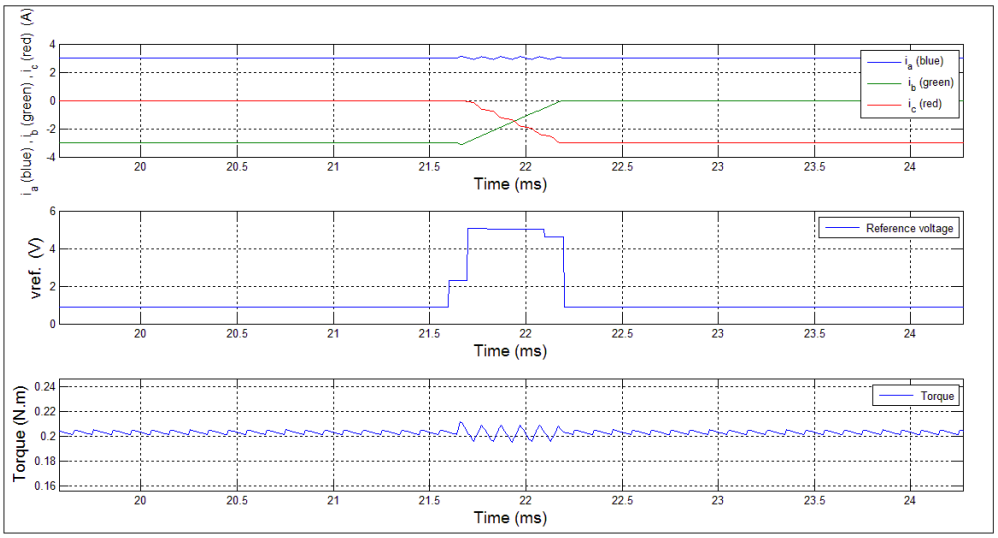

Figure 4.19: Simulation results of proposed controller for W_R = 1500 RPM

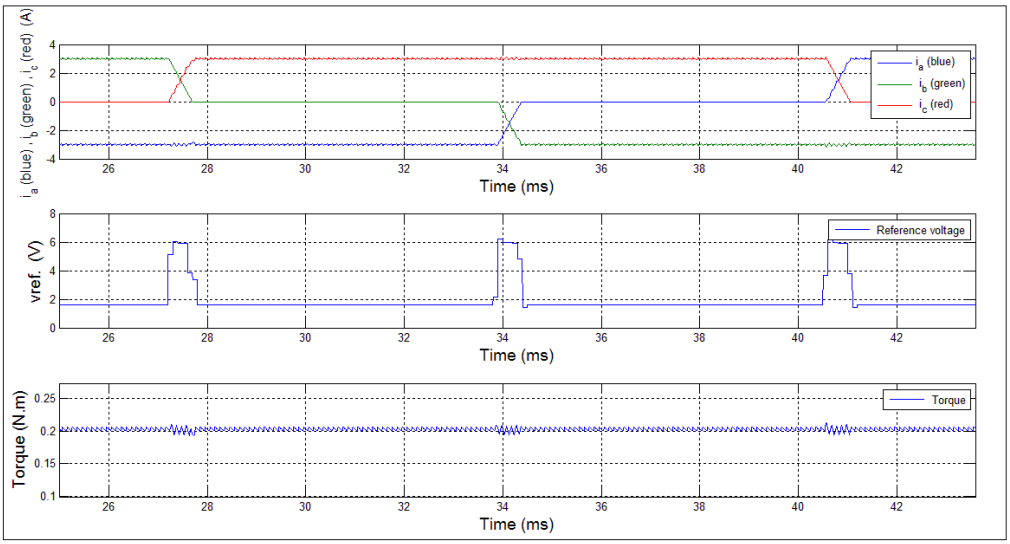

Figure 4.20: Simulation results of proposed controller for W_R= 3000 RPM

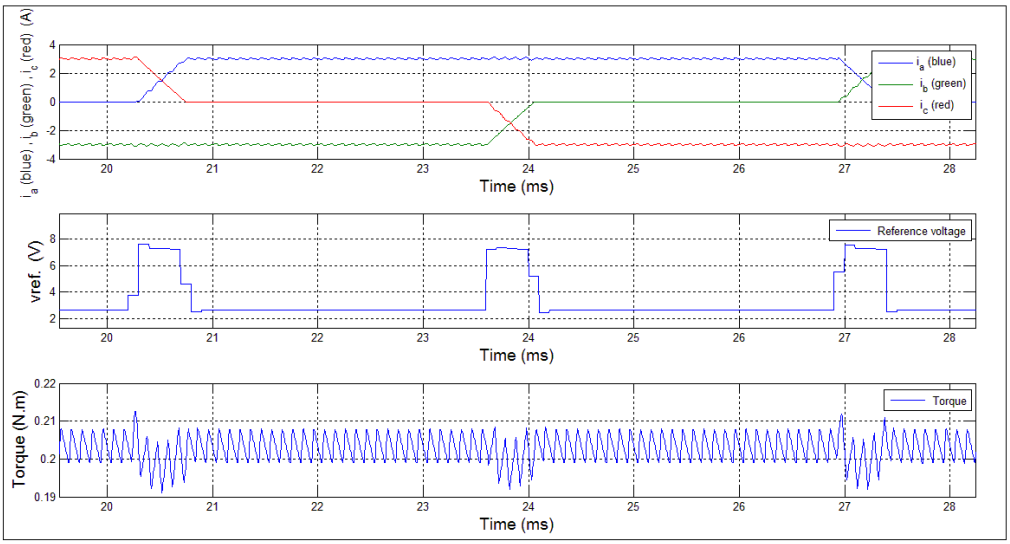

On the other hand, Figure 4.21 shows the comparison of torque response with/without proposed controller. From the torque waveform (red), it is clear to notice that high performance is achieved when proposed controller is applied.

Figure 4.21: Torque response with/without ILC for W_R = 3000 RPM

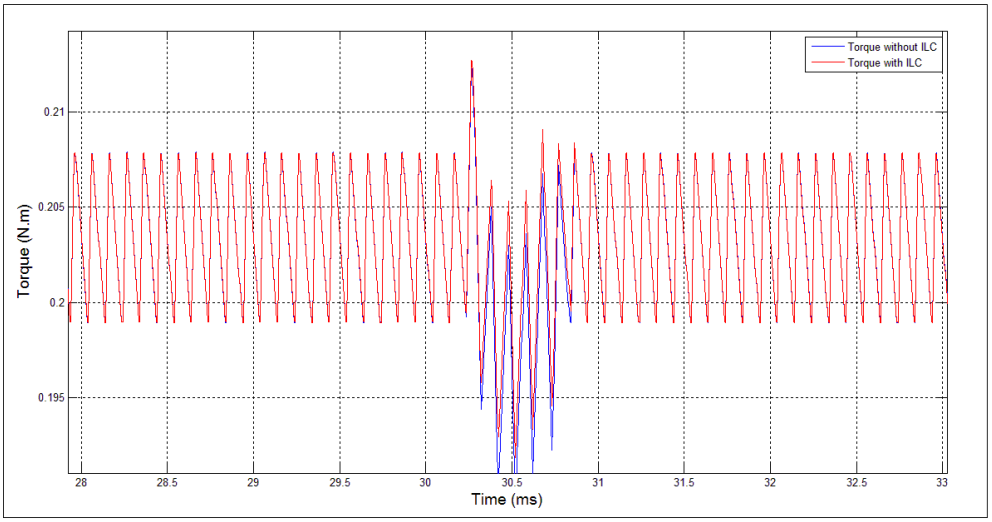

4.4 SIMULATION RESULTS WITH DIFFERENT PARAMETERS

The controller with modification of duty cycle during mixed periods and the proposed controller are tested under different parameters groups with different speeds in order to test the effectiveness of the modification of PWM during mixed periods and the proposed controller. Table 4.5 gives these parameters groups

Table 4.5: Different parameters of BLDC motor

Parameter groups	$'R$	$'L$
1	$1 * R$	$1.5 * L$
2	$1 * R$	$0.5 * L$
3	$0.5 * R$	$1.5 * L$
4	$0.5 * R$	$0.5 * L$

4.4.1 SIMULATION RESULTS OF DEAD-BEAT WITH DIFFERENT PARAMETERS

The dead-beat controller is applied with different parameter groups. Figures 4.22, 4.23 and 4.24 show the simulation results of dead-beat controller with parameters group 1 for 500 RPM, 1500 RPM and 3000 RPM respectively. From these figures, it can be seen that the results of original parameters (R =0.18Ω and L= 1.43e-3 H) are better than this case.

Figure 4.22: Simulation results of dead-beat controller for parameter group 1 and W_R = 500 RPM

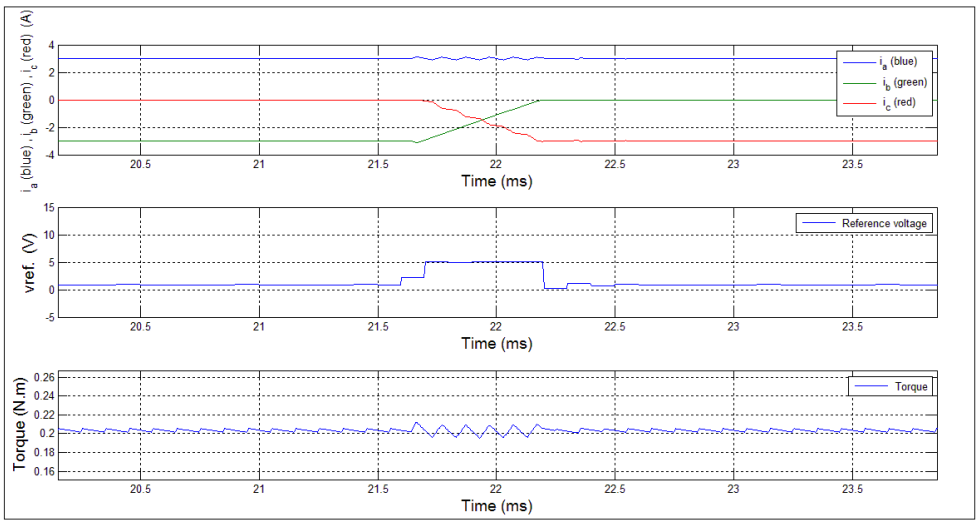

Figure 4.23: Simulation results of dead-beat controller for parameter group 1 and W_R = 1500 RPM

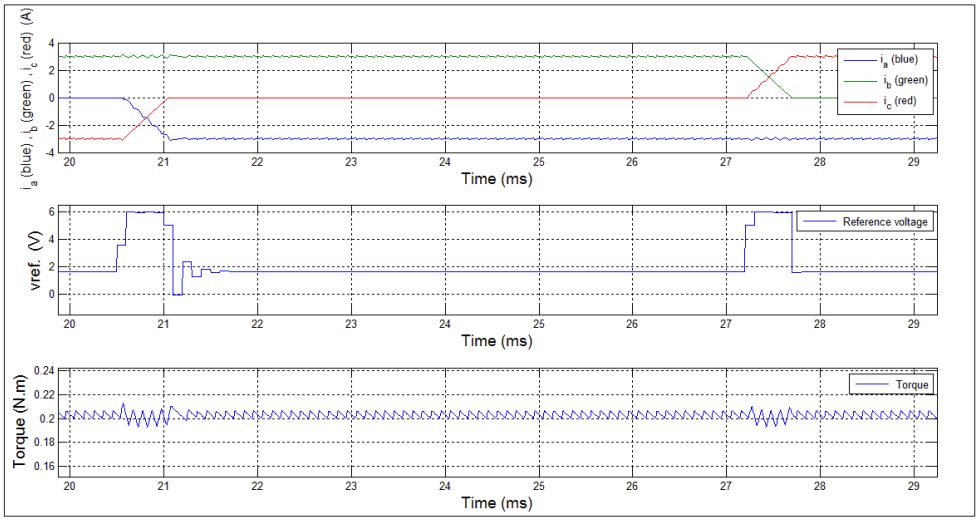

Figure 4.24: Simulation results of dead-beat controller for parameter group 1 and W_R = 3000 RPM

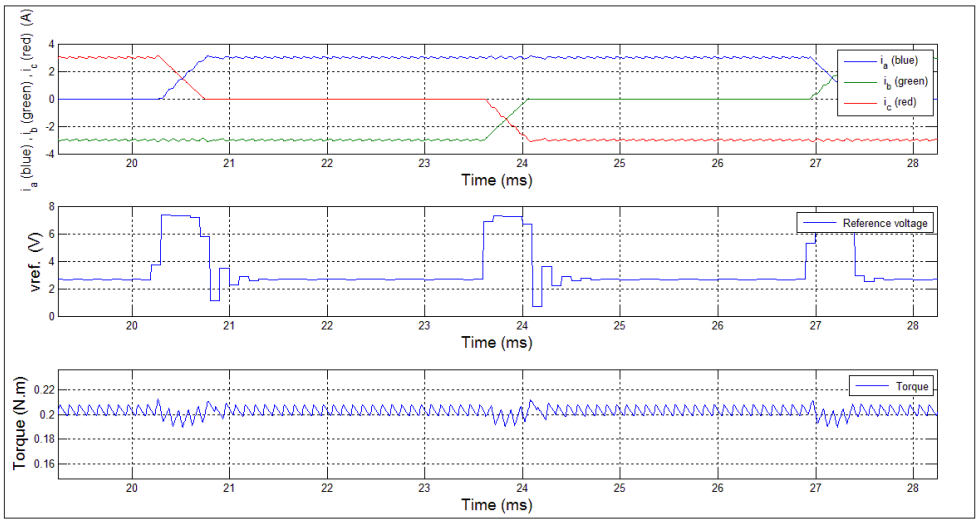

Figures 4.25, 4.26 and 4.27 show the simulation results of dead-beat controller with parameters group 2 for 500 RPM, 1500 RPM and 3000 RPM respectively, also the results are better in case of original parameter (R =0.18Ω and L= 1.43e-3 H) than this case.

Figure 4.25: Simulation results of dead-beat controller for parameter group 2 and W_R = 500 RPM

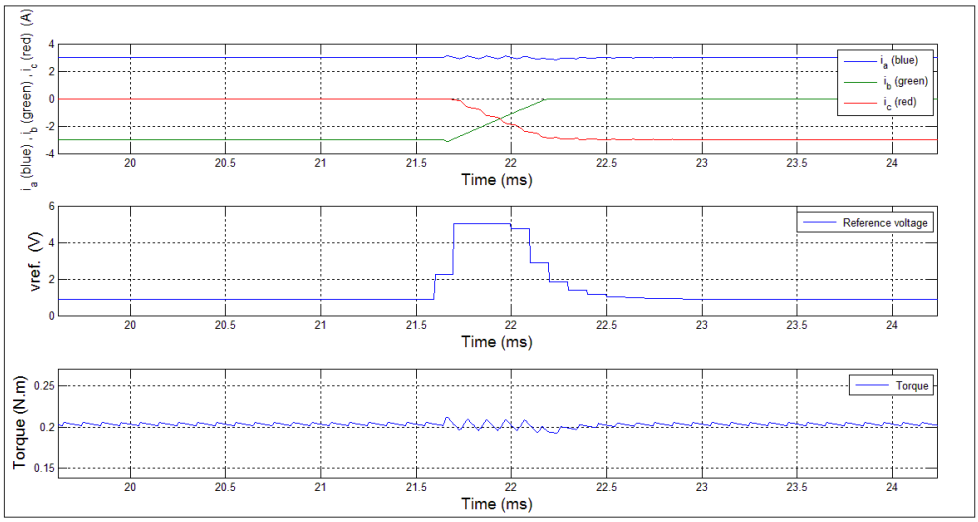

Figure 4.26: Simulation results of dead-beat controller for parameter group 2 and W_R = 1500 RPM

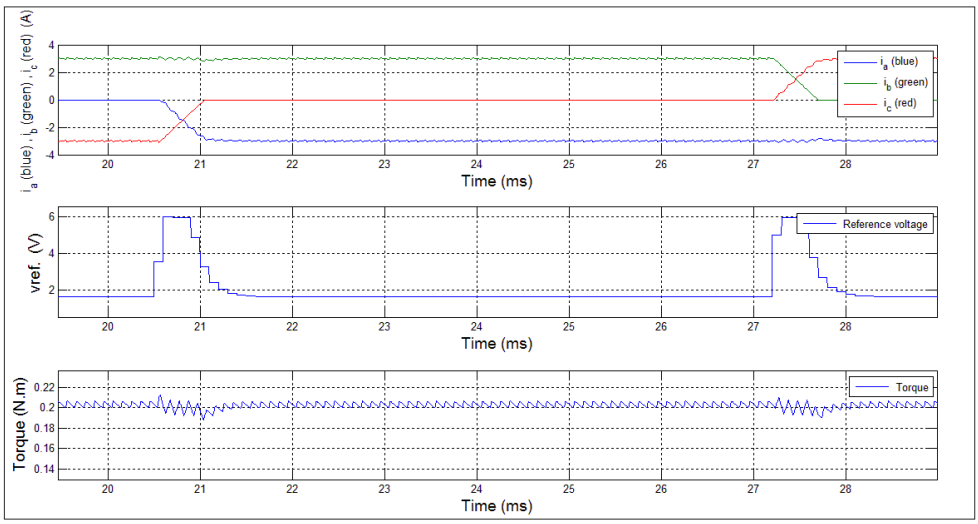

Figure 4.27: Simulation results of dead-beat controller for parameter group 2 and W_R = 3000 RPM

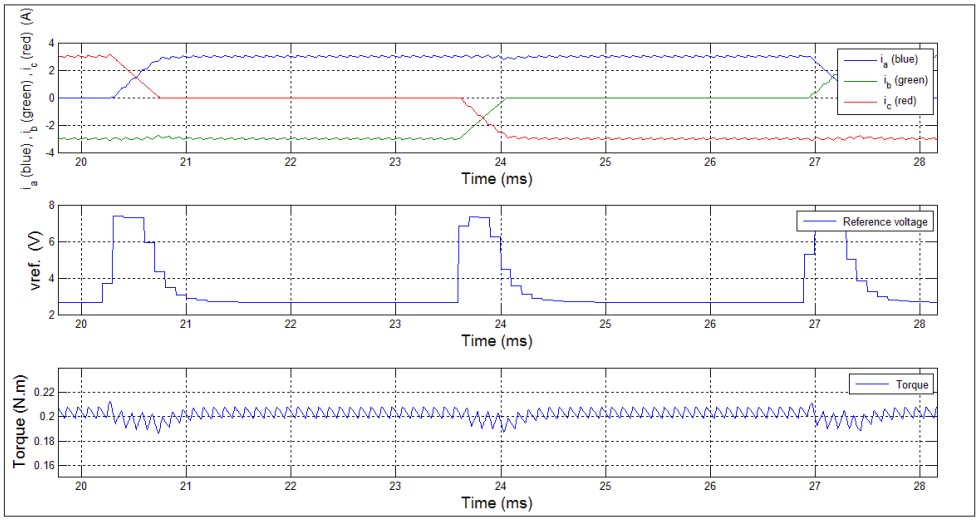

Figures 4.28, 4.29 and 4.30 show the simulation result of dead-beat controller with parameters group 3 for 500 RPM, 1500 RPM and 3000 RPM respectively. From this figures, it is obvious that a large variation in reference voltage waveform is achieved due to the change in inductance and resistance values. Because of that, there are irregular ripple in torque waveforms.

Figure 4.28: Simulation results of dead-beat controller for parameter group 3 and W_R = 500 RPM

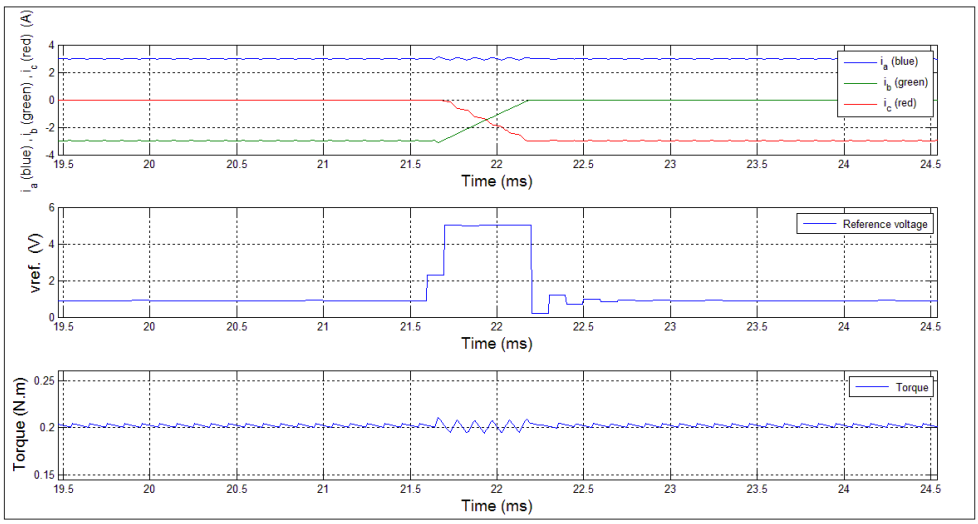

Figure 4.29: Simulation results of dead-beat controller for parameter group 3 and W_R = 1500 RPM

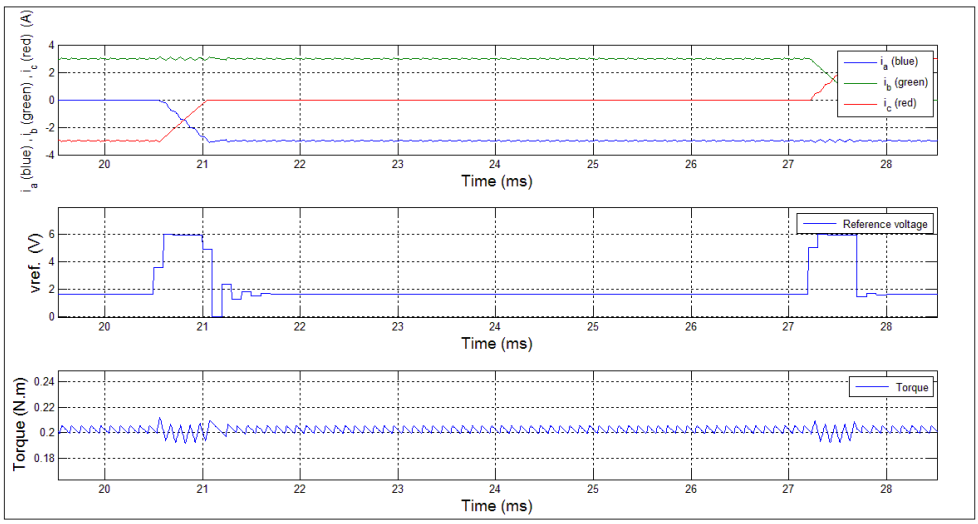

Figure 4.30: Simulation results of dead-beat controller for parameter group 3 and W_R = 3000 RPM

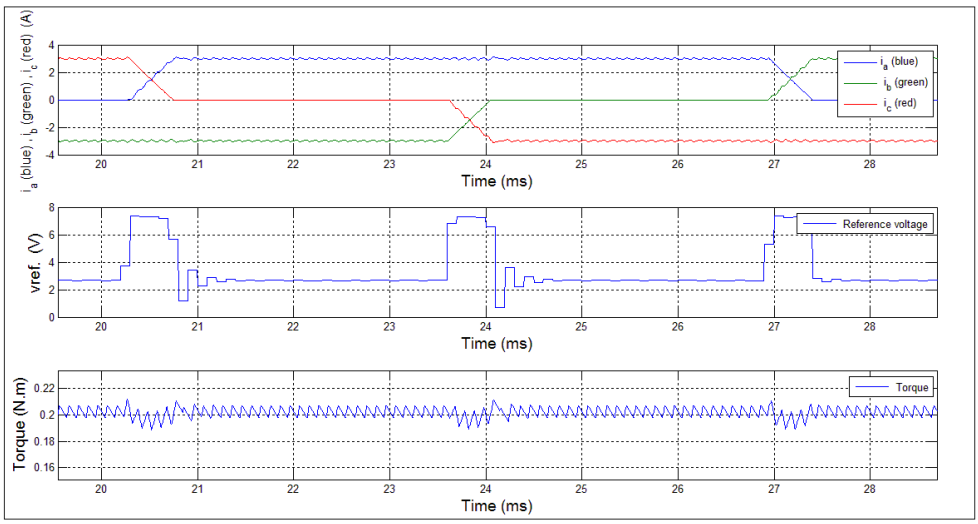

Figures 4.31, 4.32 and 4.33 show the simulation result of dead-beat controller with parameters group 4 for 500 RPM, 1500 RPM and 3000 RPM respectively. From these figures and the figures of previous parameter groups, it is obvious that a large alternation in reference voltage waveform is achieved due to the change in inductance and resistance values. Because of that, there are irregular ripples in torque waveforms. In addition, the results with original parameter groups are more efficient.

Figure 4.31: Simulation results of dead-beat controller for parameter group 4 and W_R = 500 RPM

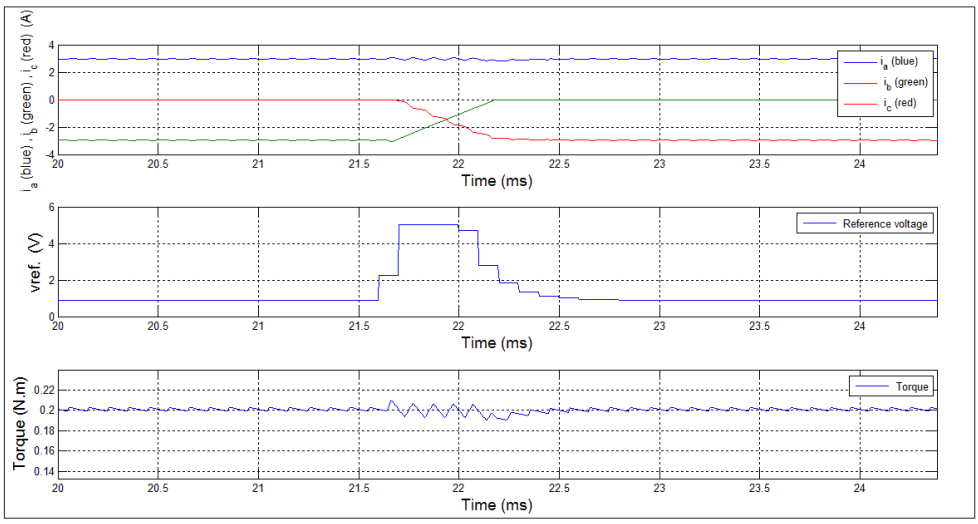

Figure 4.32: Simulation results of dead-beat controller for parameter group 4 and W_R = 1500 RPM

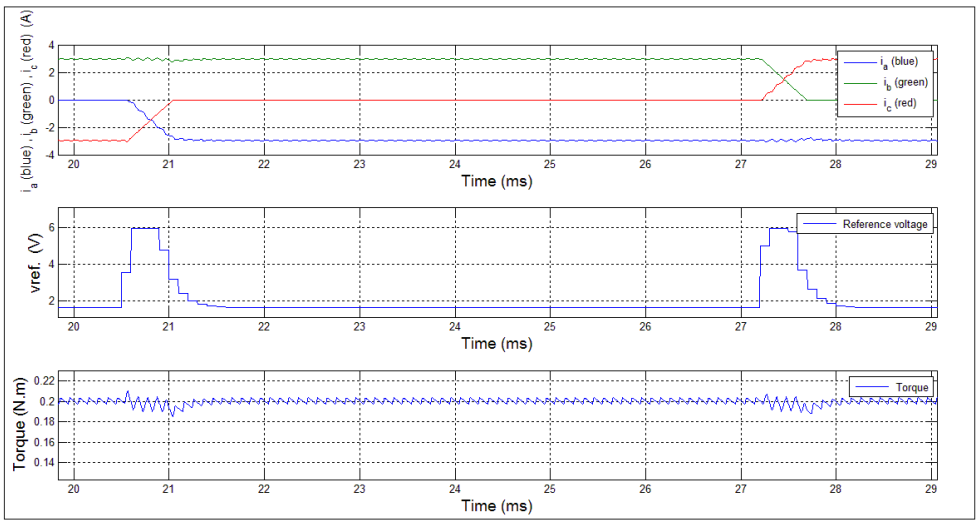

Figure 4.33: Simulation results of dead-beat controller for parameter group 4 and W_R = 3000 RPM

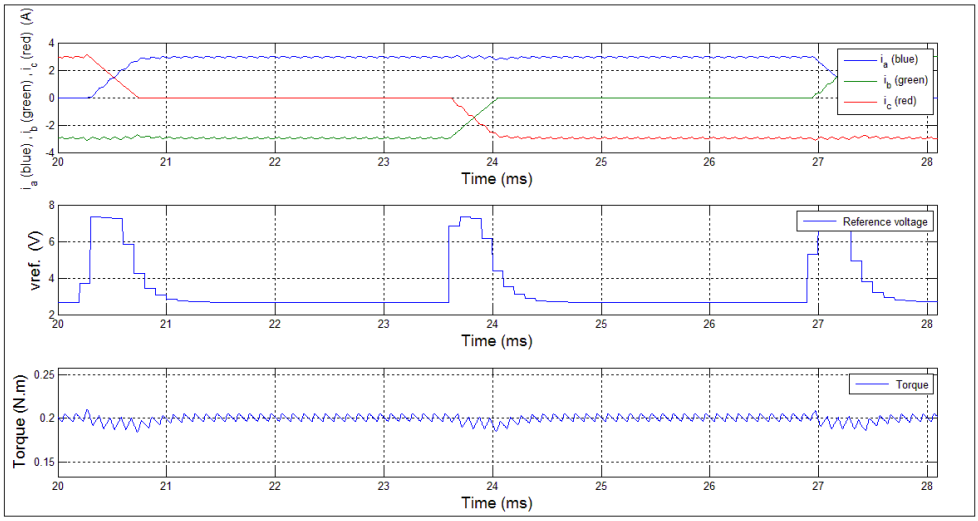

4.4.2 SIMULATION RESULTS OF PROPOSED CONTROLLER WITH DIFFERENT PARAMETERS

The proposed controller is applied with different parameters in order to confirm its effectiveness. Figures 4.34, 4.35 and 4.36 show the simulation results of proposed

controller with parameters group 1 for 500 RPM, 1500 RPM and 3000 RPM respectively.

Figure 4.34: Simulation results of proposed controller for parameter group 1 and W_R = 500 RPM

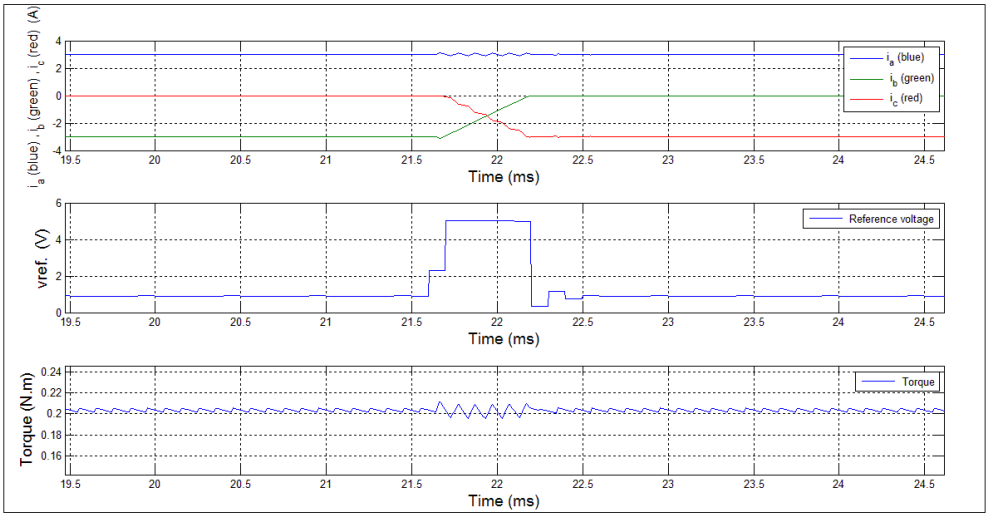

Figure 4.35: Simulation results of proposed controller for parameter group 1 and W_R = 1500 RPM

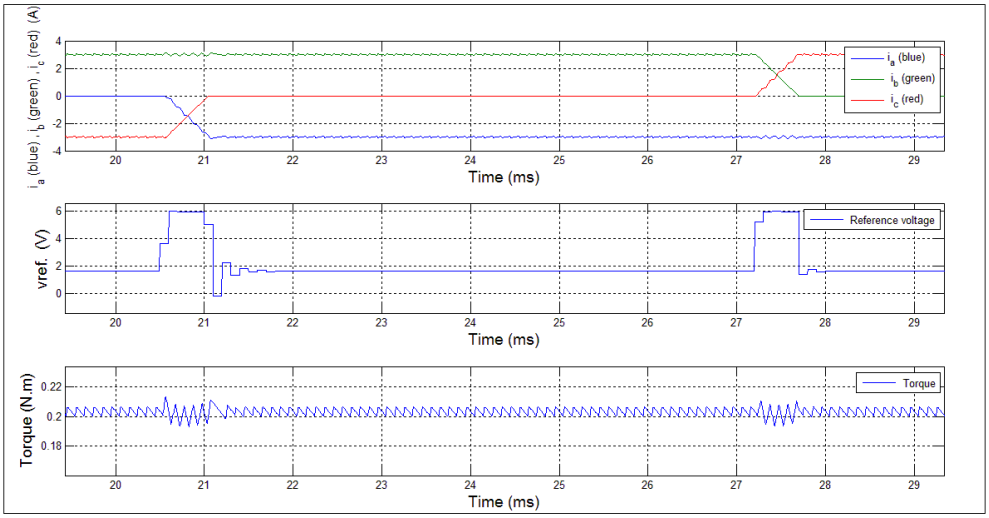

Figure 4.36: Simulation results of proposed controller for parameter group 1 and W_R = 3000 RPM

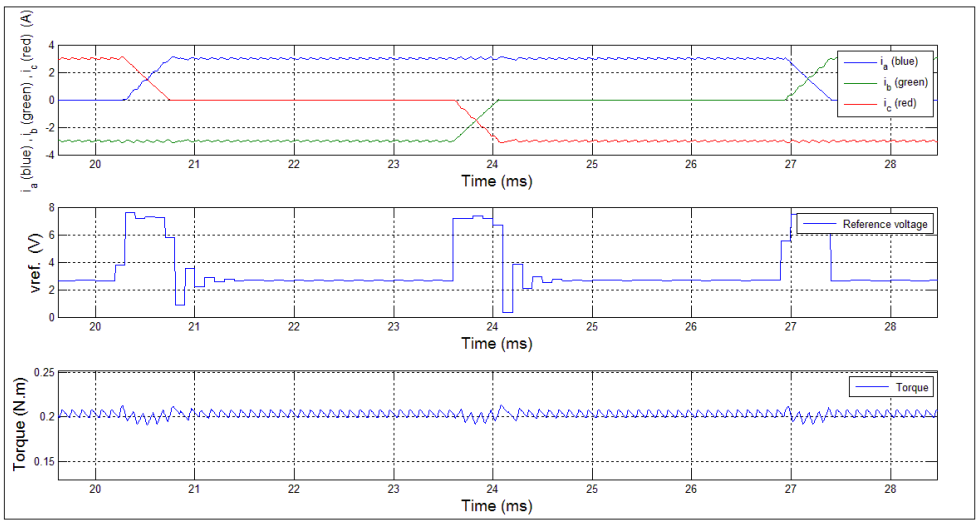

Figures 4.37, 4.38 and 4.39 show the simulation result of proposed controller with parameters group 2 for 500 RPM, 1500 RPM and 3000 RPM respectively. The results with original parameter are better than this case but this case is better than the case of just dead-beat controller is applied.

Figure 4.37: Simulation results of proposed controller for parameter group 2 and W_R = 500 RPM

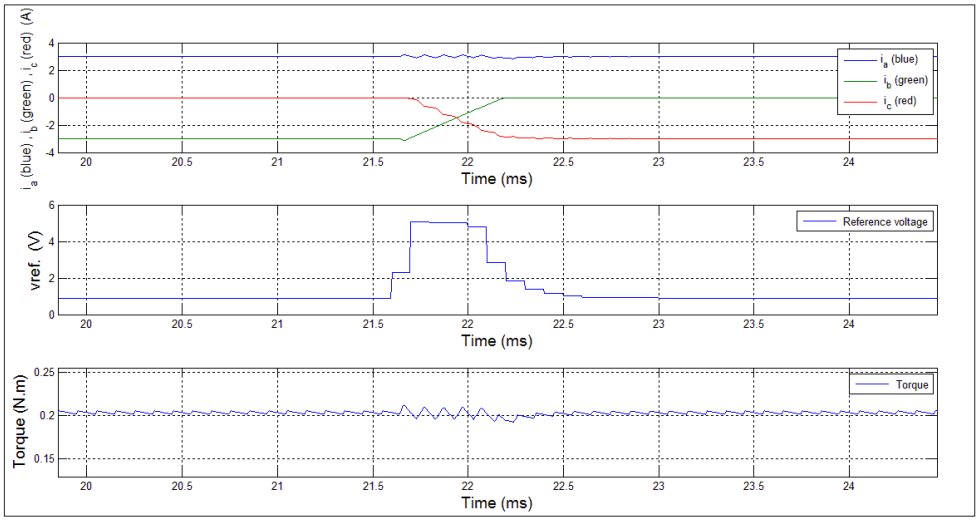

Figure 4.38: Simulation results of proposed controller for parameter group 2 and W_R = 1500 RPM

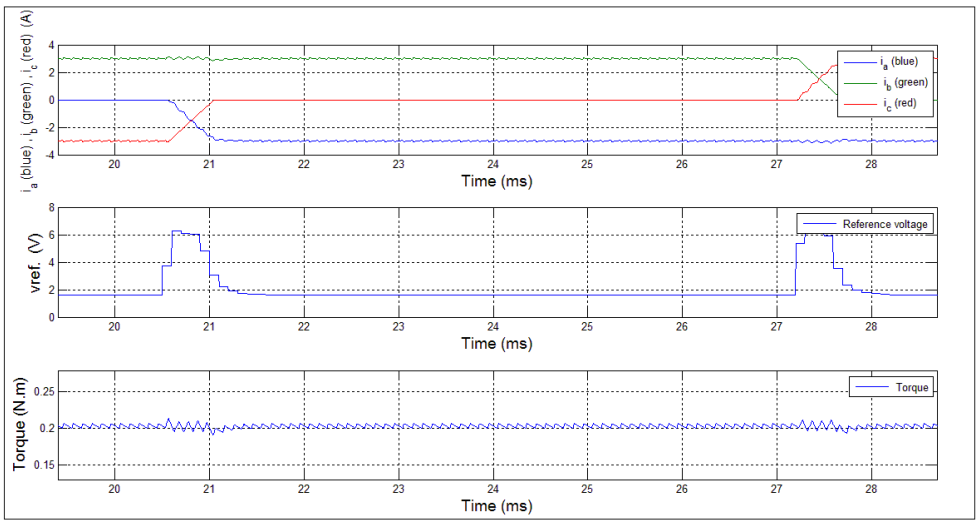

Figure 4.39: Simulation results of proposed controller for parameter group 2 and W_R = 3000 RPM

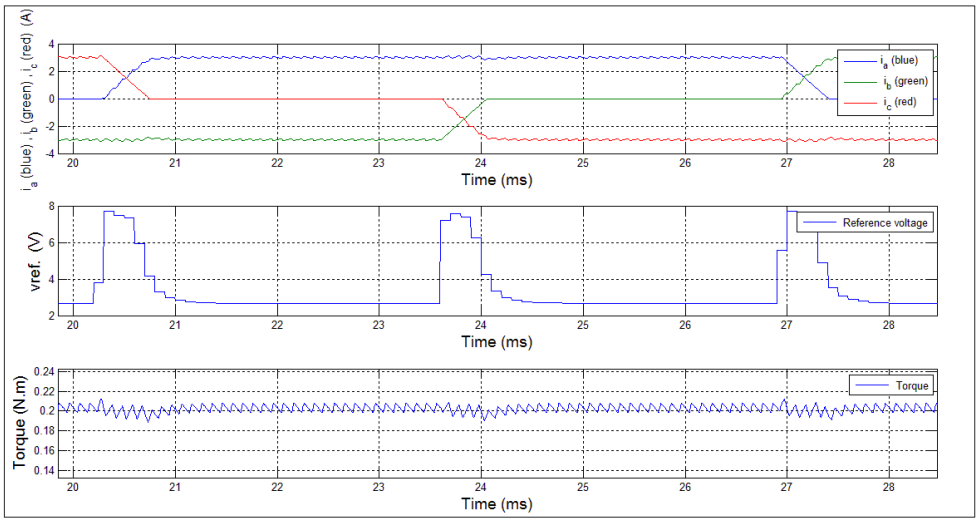

Figures 4.40, 4.41 and 4.42 show the simulation results of proposed controller with parameters group 3 for 500 RPM, 1500 RPM and 3000 RPM respectively. From these figures, it can be noticed how the maximum and minimum torque ripple are changed due to the change of reference voltage also the result with ILC is better than the case without using it.

Figure 4.40: Simulation results of proposed controller for parameter group 3 and W_R = 500 RPM

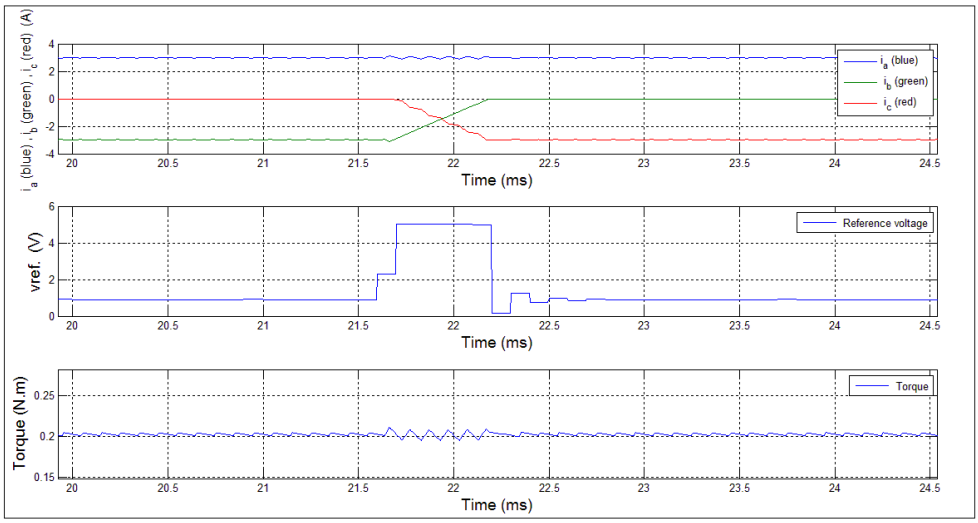

Figure 4.41: Simulation results of proposed controller for parameter group 3 and W_R= 1500 RPM

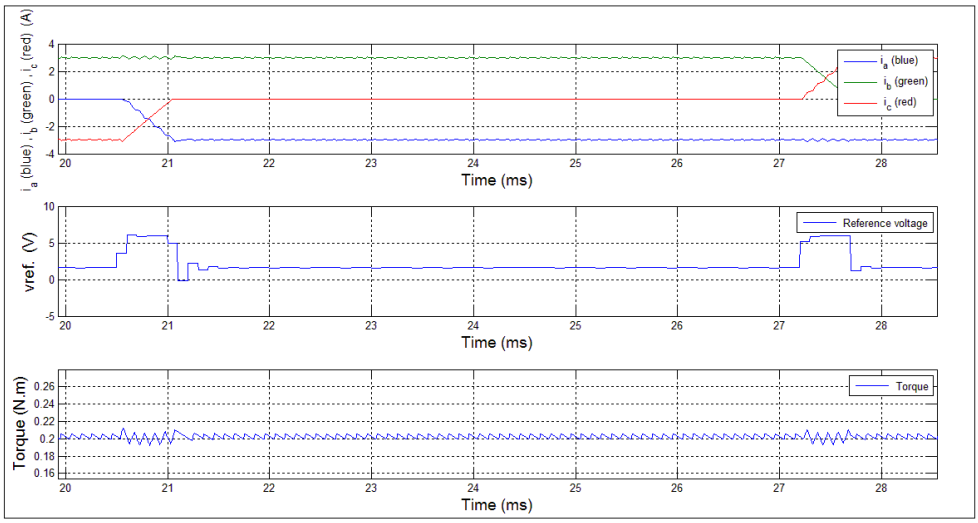

Figure 4.42: Simulation results of proposed controller for parameter group 3 and W_R = 3000 RPM

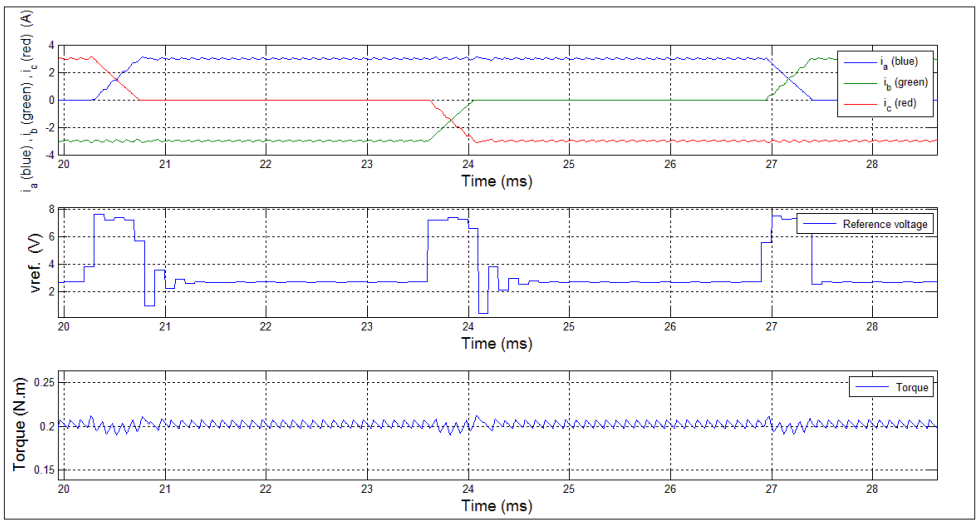

Figures 4.43, 4.44 and 4.45 show the simulation result of proposed controller with parameter group 4 for 500 RPM, 1500 RPM and 3000 RPM respectively. The results are better in case of original parameters group than this case but the results with ILC are the best.

Figure 4.43: Simulation results of proposed controller for parameter group 4 and W_R = 500 RPM

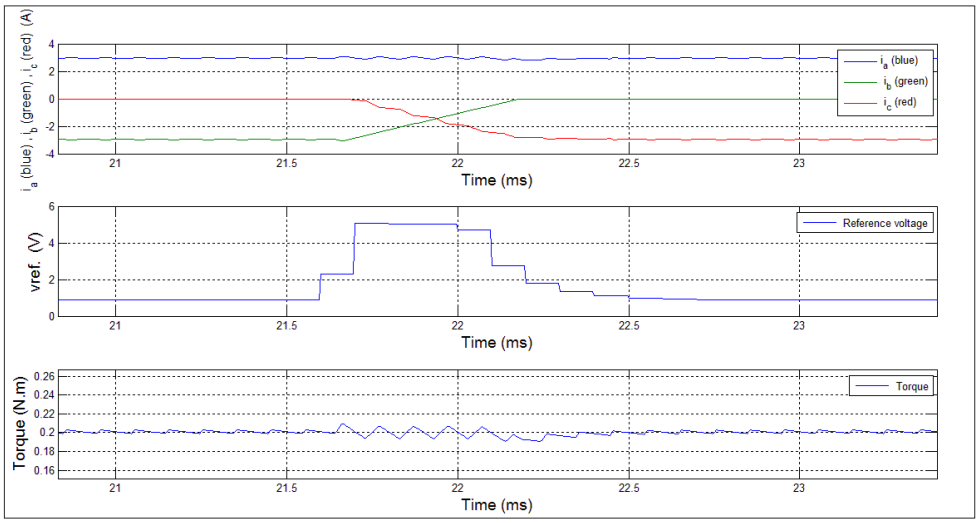

Figure 4.44: Simulation results of proposed controller for parameter group 4 and W_R = 1500 RPM

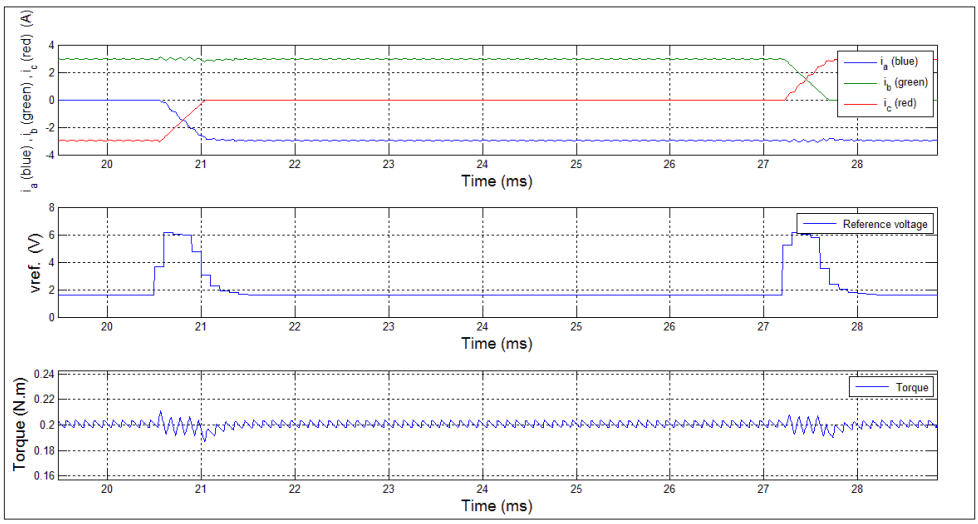

Figure 4.45: Simulation results of proposed controller for parameter group 4 and W_R = 3000 RPM

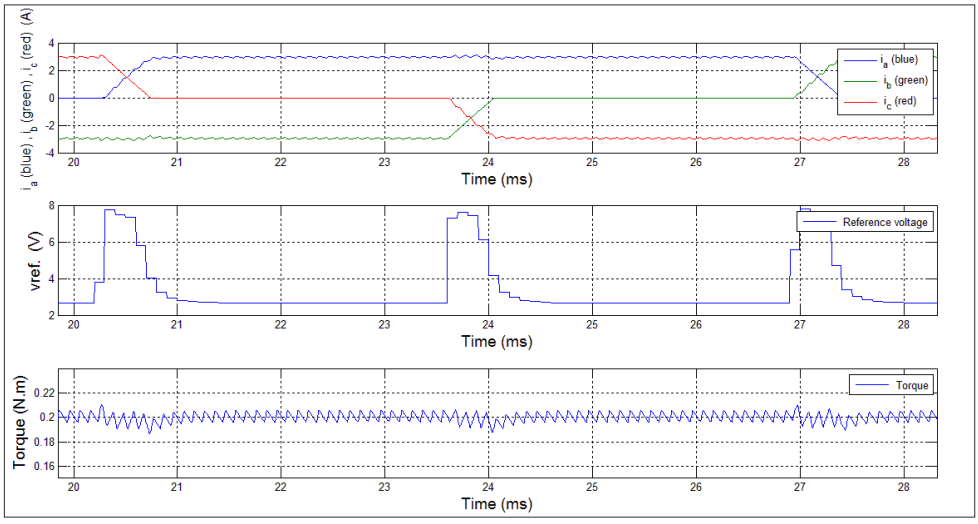

4.5 THE COMPARISON OF SIMULATION RESULTS

Tables 4.6, 4.7, and 4.8 indicate the comparison of simulations results of all simulations for 500 RPM, 1500 RPM and 3000 RPM respectively. These tables show the maximum and minimum value of un-commutation current, and torque during commutation period.

Table 4.6: The comparison of simulations results for 500 RPM

Simulations	Max. error in un-com. current	Min. un-com. current	Max. un-com. current	Max. torque error	Max. torque	Min. Torque
Dead-beat without control commutation	0.3865	2.6135	3.0089	0.0275	0.2054	0.1759
Dead-beat with control commutation	0.1709	2.8291	3.0089	0.0121	0.2100	0.1913
Dead-beat with prediction in mixed periods	0.1057	2.8956	3.1057	0.0080	0.2105	0.1954
Proposed controller	0.1044	2.8956	3.1044	0.0080	0.2105	0.1954
Dead-beat with prediction and parameters 1	0. 1053	3	3.1053	0.0080	0.2106	0.1954
Proposed controller and parameters 1	0. 1081	3	3.1081	0.0080	0.2107	0.1954
Dead-beat with prediction and parameters 2	0.1412	2.8588	3.1060	0.0100	0.2106	0.1934
Proposed controller and parameters 2	0.1399	2.8601	3.1060	0.0100	00.2106	0.1934
Dead-beat with prediction and parameters 3	0.1110	2.8890	3.0926	0.0088	0.2097	0.1946
Proposed controller and parameters 3	0.1110	2.8890	3.0926	0.0088	0.2099	0.1946
Dead-beat with prediction and parameters 4	0.1862	2.8138	3.0682	0.0130	0.2080	0.1904
Proposed controller and parameters 4	0.1856	2.8144	3.0682	0.0130	0.2082	0.1904

Table 4.8: The comparison of simulations results for 1500 RPM

Simulations	Max. error in un-com. current	Min. un-com. current	Max. un-com. current	Max. torque error	Max. torque	Min. Torque
Dead-beat without control commutation	0.4067	2.5933	3	0.0312	0.2065	0.1722
Dead-beat with control commutation	0.2773	2.7227	3	0.0210	0.2171	0.1824
Dead-beat with prediction in mixed periods	0.1451	2.8657	3.1451	0.0109	0.2130	0.1925
Proposed controller	0. 1549	2.8657	3.1549	0.0103	0.2136	0.1931
Dead-beat with prediction and parameters 1	0.1462	2.8845	3.1462	0.0109	0.2130	0.1925
Proposed controller and parameters 1	0.1530	2.8845	3.1530	0.0105	0.2135	0.1931
Dead-beat with prediction and parameters 2	0.2352	2.7648	3	0.0160	0.2130	0.1874
Proposed controller and parameters 2	0.2346	2.7654	3	0.0158	0.2136	0.1876
Dead-beat with prediction and parameters 3	0.1334	2.8678	3.1334	0.0117	0.2122	0.1917
Proposed controller and parameters 3	0.1426	2.8678	3.1426	0.0114	0.2128	0.1920
Dead-beat with prediction and parameters 4	0.2611	2.7389	3	0.0181	0.2105	0.1853
Proposed controller and parameters 4	0.2556	2.7444	3	0.0174	0.2112	0.1860

Table 4.9: The comparison of simulations results for 3000 RPM

Simulations	Max. error in un-com. current	Min. un-com. current	Max. un-com. current	Max. torque error	Max. torque	Min. Torque
Dead-beat without control commutation	0.4252	2.5748	3	0.0356	0.2079	0.1678
Dead-beat with control commutation	0.2935	2.7065	3.0007	0.0243	0.2197	0.1791
Dead-beat with prediction in mixed periods	0.1500	2.8500	3.1374	0.0139	0.2125	0.1895
Proposed controller	0.1708	2.8604	3.1708	0.0133	0.2155	0.1901
Dead-beat with prediction and parameters 1	0.1374	2.9344	3.1374	0.0140	0.2112	0.1894
Proposed controller and parameters 1	0. 1773	2.9344	3.1773	0.0135	0.2136	0.1899
Dead-beat with prediction and parameters 2	0.2364	2.7636	3.1035	0.0170	0.2113	0.1846
Proposed controller and parameters 2	0.2225	2.7775	3.1035	0.0164	0.2129	0.1870
Dead-beat with prediction and parameters 3	0.1383	2.8617	3.1250	0.0147	0.2104	0.1887
Proposed controller and parameters 3	0.1670	2.8686	3.1670	0.0143	0.2130	0.1891
Dead-beat with prediction and parameters 4	0.2832	2.7168	3	0.0196	0.2087	0.1838
Proposed controller and parameters 4	0.2671	2.7329	3	0.0190	0.2134	0.1844

5. DISCUSSION AND CONCLUSION

Torque characteristics of brushless DC motor drives indicate the commutation torque ripple is major reason restricting the usage of BLDC motors in application requiring higher performance. Moreover, the torque ripple during the commutation is about 50% of the average torque (Zhang, 2014). The dynamical models of BLDC motors are nonlinear, because of that the conventional controller are not suitable. Therefore, in this thesis, commutation torque ripple reduction method has been proposed by using iterative learning controller in conjunction with dead-beat controller.

ILC is implemented during commutation period to provide the additional compensation reference voltage. This implementation is simple to do because ILC can be added to any control system without remodeling the whole control system. The characteristics of this controller are evaluated by numerical simulation. Moreover, the Simulation results are presented with different cases:

1. Dead-beat controller without control commutation
2. Dead-beat controller with control commutation
3. Dead-beat controller with control mixed periods
4. Proposed controller
5. Dead-beat controller with control mixed periods for different parameters groups
6. Proposed controller for different parameters groups

The Simulation results are reported as figures and tables in chapter 4. From these tables and all figures, it can be seen and concluded that, the torque ripple is low for 500rpm comparing to the high speed, and the spikes and dips (ripple) of un-commutated current are appeared due to the commutation. Because of that, the torque is affected by appearing the ripple in its waveform.

When proposed controller is employed during commutation period, the un-commutated current ripples are attenuated for all simulation cases as in the comparison tables. Consequently, the commutation torque ripple is suppressed. Therefore, these results

proved the effectiveness of proposed controller, because the resulting torque has lower torque ripple for all cases. The performance of proposed controller is tested with different motor parameter groups and the results with ILC are better without using it. Thus, the proposed controller is suitable for wide range of motor parameter groups because the torque ripple is the lowest for all cases when ILC is applied. Moreover, ILC is appropriate of full range speed.

6. REFERENCES

1. Ahn, H-S., Chen, Y. Q. and Moore K. L., "*Iterative Learning Control: Brief Survey and Categorization",* IEEE Transaction on Systems, Man, and Cybernetics – part C: Applications and VOL. 37, NO. 6, NOVEMBER 2007
2. Ahn, H., Moore, K. and Chen, Y. *"Stability analysis of iterative learning control system with interval uncertainty"*, *IFAC,* 2005.
3. Anand, K., Sathishkumar, V., Jagadeeshwaran, A., Periyasamy, V. M., "*Analysis of torque ripple and speed control of five phase BLDC motor*", International Conference on Innovation in Science Engineering, Technology and Management, 2014.
4. Atmel AVR443, *"Sensor-based Control of Three Phase Brushless DC Motor"*, Atmel Corporation, www.atmel.com, 2013.
5. Atmel Corporation, "*Brushless dc motor using* ATmega32, www.atmel.com", 2008.
6. Berendsen, C-S., "Champenois, G.C., and Bolopion, M., "*Commutation Strategies for Brushless DC Motors: Influence on Instant Torque",* IEEE Transactions on Power Electronics, VOL. 8, NO. 2, APRIL 1993
7. Bharatkar, S.S., Chatterjee, D. Yanamshetti, R. and Ganguli,A.K. ,"*Commutation Torque Ripple Analysis and Reduction Through Hybrid Switching for BLDC Motor Drives*", IEEE 2008.
8. Bristow, D. A., Tharayil, M. and Alleyne, A. G., *"*A *survey of alterative learning control from IEEE control system",* IEEE Control System Magazine JUNE 2006.
9. Brown, W.,*" Brushless DC Motor Control Made easy*", Microchip Technology Inc., 2002.
10. Carlson, R., Lajoie-Mazenc, M. and Fagundes, and J. C.,*"Analysis of Torque Ripple Due to Phase Commutation in Brushless dc Machines,"* IEEE Transaction on Industry Applications, VOL. 28, NO. 3, MAY/JUNE 1992.
11. Doh, T.-Y., Ryoo, J.R. and Chung M.J., *"Design of a repetitive controller: an application to the track-following servo system of optical disk drives"*, IEEE Proc.-Control Theory Appl., Vol. 153, No. 3, May 2006.
12. Elevich, L. N.,"*3 phase BLDC motor control with hall sensors using 56800/E digital signal controller",* Free scale Semiconductor, Inc., 2005.
13. Eriksson, P., "*Design and implementation of a servo system by Sensor Field Oriented Control of a BLDC motor",* UPTEC F 14051, 2014.
14. Giessen, C.V., Zou, Q., and Devasia, S.,*"Inversion-based Precision-Positioning of Switching Inertial Reaction Devices",* In Proceeding of American control conference, 2004.

15. Hunter, K. J., Sbarbaro, D., Żbikows, R., Gawthrop, P. J., *"Neural networks for control systems to survey",* available online 11 February 2003.
16. Hara, S., Yamamoto, Y., Omata, T., and Nakano, M., "*Repetitive control system: a new type servo system for periodic exogenous signals*", IEEE Trans. Automat. Control, 37, (7), pp. 659-668 1988.
17. Kim, D. I., and Kim, S.,"*An iterative learning control method with application for CNC machine tools",* Industry Applications, IEEE Transaction on Industry Applications, VOL.32, NO.1, 1996.
18. Keeping, S., "*Controlling Sensor less, BLDC Motors via Back EMF",* Contributed By Hearst Electronic Products 2013.
19. Krishnan, R., *Permanent Magnet Synchronous and Brushless DC Motor Drives*, Taylor & Francis Group 6000 Broken Sound Parkway NW, U.S.A, 2010.
20. Lam, B., Panda, SK., and Xu, J.-X. ," *Reduction of Periodic Speed Ripples in PM Synchronous Motors using Iterative Learning Control*," IEEE 2000.
21. Le-Huy, H., Perret, R. and Feuillet, R, "*Minimization of Torque Ripple in Brushless DC Motor Drives*", IEEE Transaction on Industry Applications, VOL. IA-22, NO. 4, JULY/AUGUST 1986.
22. Lee, E. C.," *Application of brushless DC in blow molding*", Powertec Industrial Corporation. http://powertecmotors.com/ablowe2.pdf, No date.
23. Lee, S., Lemley, T., and Keohane, G., "*comparison study of the commutation methods for the three-phase permanent magnet brushless DC motor".* http://www.magnelab.com/wp-content/uploads/2015/02/A-comparison-study-of-the-commutation-methods-for-the-three-phase-permanent-magnet-brushless-dc-motor.pdf. No date,
24. Lee, J. T., Ribeiro, C., and Mendoza, M., *Designing High-Performance and Power Efficient 3-Phase Brushless DC Motor Control Systems*, Micrel, Inc., 2014.
25. Lin, H., Yan, W., Yao, Y., and Gao, B. ,"*Robust nonlinear speed control for a brushless DC motor using model reference adaptive backstepping approach",* IEEE 2009.
26. Lu, H., Zhang, L., and Qu, W., "A *New Torque Control Method for Torque Ripple Minimization of BLDC Motors with Un-Ideal Back EMF* ", IEEE Transactions on Power Electronics, VOL. 23, NO. 2, MARCH, 2008.
27. Ma, T.-T., Lee, M.- H., *"Design of fuzzy based iterative learning controllers for induction motor drives, Power Electronics and Drive Systems",* Power Electronics and Drive Systems, Publications IEEE 2009.
28. Moore, K., Johnson, M., and Grimble, M.*," Iterative Learning Control for Deterministic Systems",* Springer-Verlag New York, Inc. Secaucus, NJ, USA ©1993
29. Oguntoyinbo, O. J., *PID control of brushless dc motors and robot trajectory planning and simulation with matlab/simulink*, Programed degree of information degree, University of Applied Sciences, 2009.
30. Padmaraja, Y., *Brushless dc motor fundamental*, Microchip Technology Inc., 2003.

31. Panda, S. K., Xu, J.-X.and Qian, W., "Review of Torque Ripple Minimization in PM Synchronous Motor Drives," IEEE 2008.
32. Park, S. J., Park, H. W., Lee, M. H., and Harashima, F., "A *new Approach for Minimum-Torque-Ripple Maximum-Efficiency Control of BLDC Motor",* IEEE Transactions on Industrial Electronics, VOL. 47, NO. 1, FEB RUARY, 2000.
33. Quan, W., Ling, Z., and Chao, F. "*Research on deadbeat Current Control Strategy of Three-Phase PWM Voltage Source Rectifier* ", ICCSEE 2013
34. Qian, W., Panda, S. K., " *Speed Ripple Minimization in PM Synchronous Motor Using Iterative Learning Control",* IEEE Transaction on Energy Conversion, VOL. 20, NO. 1, MARCH 2005.
35. Salah, W. A., Ishak, D., Hammadi, K. J., "*minimization of torque ripples in BLDC motor due to phase commutation",* Przeglad Electrotechiczny (Electrical Review), ISSN 0033-2097, R. 87 NR 1/2011.
36. Salah, W. A., Ishak, D., Hammadi, K. J., *PWM switching strategy for torque ripple minimization in BLDC motor* ", Journal of Electrical Engineering , VOL.
37. Salah, W. A., Ishak, D., Abu Zneid, B., Abu_Al_Aish, A, Jadin, M.,and Abu Sneineh, A, "*Implementation of PWM control strategy for torque ripples reduction in brushless DC motor",* Springer-Verlag Berlin Heidelberg 2015.
38. Shi, J., Li, T. - C., "*New Method to Eliminate Commutation Torque Ripple of Brushless DC Motor with Minimum Commutation Time*", IEEE Transaction on Industrial Electronics, VOL. 60, NO. 6, JUNE 2013.
39. Song, J.-H., Choy, I., "*Commutation Torque Ripple Reduction in Brushless DC Motor Drives Using a Single DC Current Sensor*", IEEE Transactions on Power Electronics, VOL. 19, NO. 2 MARCH 2004.
40. Swevers, J. *"Iterative Learning Control (ILC) [H04Q7]*" http://people.mech.kuleuven.be/~jswevers/course_vub/slides/ilc.pdf 2014.
41. Yuan, Y., Auger, F., and Loron, L.,"*Design of a Lying Sensor for Permanent Magnet Synchronous Machine Torque Ripple Reduction using the Iterative Learning Control Technique",* IEEE 2011.
42. Zhang, J., Chen, S., and Liu, L. *"Research on commutation torque ripple suppression strategy of BLDCM based on iterative learning"* COMPUTER MODELLING & NEW TECHNOLOGIES 18(5) 288-296 2014.